Inorg. Chem. **2008**, *47*, 9279−9292

Synthesis and Characterization of the Trihalophosphine Compounds of Ruthenium [$RuX_2(\eta^6$-cymene)(PY_3)] (X = Cl, Br, Y = F, Cl, Br) and the Related $PF_2(NMe_2)$ and $P(NMe_2)_3$ Compounds; Multinuclear NMR Spectroscopy and the X-ray Single Crystal Structures of [$RuBr_2(\eta^6$-cymene)(PF_3)], [$RuBr_2(\eta^6$-cymene)$(PF_2\{NMe_2\})$], and [$RuI_2(\eta^6$-cymene)$(P\{NMe_2\}_3)$]

Ahmed M. A. Boshaala,[†] Stephen J. Simpson,*[,†,‡] Jochen Autschbach,*[,§] and Shaohui Zheng[§]

Institute of Materials Research, University of Salford, Salford M5 4WT, U.K., School of Biosciences, University of Exeter, 216B Geoffrey Pope Building, Stocker Road, Exeter EX4 4QD, U.K., and Department of Chemistry, 312 Natural Sciences Complex, State University of New York at Buffalo, Buffalo, New York 14260-3000

Received April 4, 2008

Treatment of the dimers [$RuX_2(\eta^6$-cymene)$]_2$ with PF_3 in hot heptane produces the compounds [$RuX_2(\eta^6$-cymene)(PF_3)] (X = Cl, Br, I) in good yield. Difluoro(dimethylamino)phosphine and tris(dimethylamino)phosphine react similarly to produce the compounds [$RuX_2(\eta^6$-cymene)$(PF_2\{NMe_2\})$] and [$RuX_2(\eta^6$-cymene)$(P\{NMe_2\}_3)$]. Reaction of the dimers [$RuX_2(\eta^6$-cymene)$]_2$ with PCl_3 and PBr_3 proceeded with the production of mononuclear products which had undergone halogen exchange at ruthenium in some cases. ^{1}H, ^{13}C, ^{31}P, and ^{19}F NMR spectra have been obtained where appropriate together with (^{1}H−^{1}H) correlation spectroscopy (COSY) and (^{13}C−^{1}H)-HETCORR spectra of selected compounds. The variation of $^1J(^{31}P-^{19}F)$ with the nature of the auxiliary ligand (X) in the PF_3 and $PF_2(NMe_2)$ complexes has been examined both experimentally and computationally using a natural localized molecular orbital-natural bond order approach. The single crystal X-ray structure of [$RuBr_2(\eta^6$-cymene)(PF_3)] has been determined at 223 K and those of [$RuBr_2(\eta^6$-cymene)$(PF_2\{NMe_2\})$] and [$RuI_2(\eta^6$-cymene)$(P\{NMe_2\}_3)$] at 294 K.

Introduction

The preparative transition metal chemistry of trifluorophosphine (PF_3) blossomed in the period 1960−1985 with the work of Clark,[1] Kruck,[2] and Nixon.[3,4] The volatility of many homoleptic derivatives has been used in mass transfer applications, for example, the use of [$Fe(PF_3)_5$] to determine isotope ratios in iron samples[5] and deposition of platinum films from [$Pt(PF_3)_4$].[6] The PF_3 ligand has very similar π-acceptor properties to carbon monoxide, the respective Tolman electronic parameters are 2111 cm^{-1} and 2128 cm^{-1}, the latter value being obtained from the Raman spectrum of $Ni(CO)_4$.[7] Trifluorophosphine compounds are comparatively less common; this could be due to the coordinated ligand being an insensitive infrared probe and the very high commercial cost of the gas compared to carbon monoxide. The free ligand has a reputation for being much more toxic than carbon monoxide, both are colorless and odorless but whereas the symptoms of carbon monoxide poisoning are pinkness of complexion, drowsiness, and eventual loss of consciousness, the phosphine causes sharp chest pains, nausea, and weakness on inhalation of small quantities.[8−10]

* To whom correspondence should be addressed. E-mail: s.j.simpson@exeter.ac.uk. (S.J.S.), jochena@buffalo.edu (J.A.).
† University of Salford.
‡ University of Exeter.
§ State University of New York at Buffalo.

(1) Clark, R. J.; Busch, M. A. *Acc. Chem. Res.* **1973**, *6*, 246–252.
(2) Kruck, T. *Angew. Chem., Int. Ed. Engl.* **1967**, 53–67.
(3) Nixon, J. F. *Endeavour* **1973**, *32*, 19–24.
(4) Nixon, J. F. *Adv. Inorg. Chem.* **1985**, *29*, 41–141.
(5) Taylor, P. D. P.; Lehto, S.; Valkiers, S.; De Bievre, P.; Selgrad, O.; Flegel, U.; Kruck, T. *Anal. Chem.* **1998**, *70*, 1033–1035.
(6) Wang, S.; Sun, Y. M.; Wang, Q.; White, J. M. *J. Vac. Sci. Technol. B.* **2004**, *22*, 1803–1806.
(7) Stammreich, H.; Kawai, K.; Sala, O.; Krumholz, P. *J. Chem. Phys.* **1961**, *35*, 2168–2174.
(8) Booth, H. S.; Frary, S. G. *J. Am. Chem. Soc.* **1939**, *61*, 2934–2937.

10.1021/ic800611h CCC: $40.75
Published on Web 09/23/2008

Both gases cause a pronounced rise in body temperature in small doses, but there are no comparative human toxicity data for the pair. Trifluorophosphine is known to form a complex with hemoglobin which is rapidly hydrolyzed under physiological and alkaline conditions.[11] Our aim was to generate PF_3 as required and to investigate the NMR spectroscopic properties of the ligand attached to a ruthenium center.

The coordination chemistry of the other phosphorus trihalides is more limited due partially to the poorer ligating properties and more commonly to the extreme moisture sensitivity of both the ligands and the metal compounds prepared. Phosphorus trifluoride is only hydrolyzed slowly in mildly acidic and neutral solutions. Schutzenberger[12] obtained a stable complex of PCl_3 with $PtCl_2$ in the nineteenth century, and in the early period of development of the Dewar−Chatt−Duncanson bonding model, stable nickel compounds of PCl_3 and PBr_3 were reported.[13−15] This work was later extended with the advent of multinuclear NMR spectrometry.[16] A number of Group 6 metal compounds $[M(CO)_5(PX_3)]$ have been prepared, structurally characterized, and investigated theoretically; these include PF_3, PCl_3, and PBr_3 compounds.[17,18] Earlier we prepared the carbonyl compound $[RuCl_2(\eta^6\text{-cymene})(CO)]$,[19] and the stability of this compound containing a poor σ- donor ligand directed us to prepare series of related compounds containing these three halophosphine ligands.

Results and Discussion

Complexes of PF_3 and $PF_2(NMe_2)$. The laboratory scale generation of trifluorophosphine (bp −101 °C) usually involves the reaction of phosphorus trichloride (bp 76 °C) with either hydrogen fluoride gas,[10] antimony trifluoride,[20] arsenic trifluoride,[21] or zinc fluoride.[22] These reactions are stepwise replacements, and the residence time in the reaction zone is critical in controlling the extent of replacement. Contamination with the mixed products $PFCl_2$ (bp 14 °C) and PF_2Cl (bp −47 °C) is a potential problem in each case because of the inconvenient boiling points and necessitates careful control of reaction conditions and product distillation. We decided to modify this Swarts reaction approach by reacting phosphorus tribromide (bp 175 °C) with antimony trifluoride in the absence of acetonitrile which is normally used as a solvent; Booth and Frary[8] explored this reaction in detail, and the byproducts $PFBr_2$ (bp 78 °C) and PF_2Br (bp −16 °C) are much easier to remove. Furthermore, PF_2Br is not very stable under the reaction conditions and disproportionates to PBr_3 and PF_3. In our hands the reverse addition of the PBr_3 to solid SbF_3 and simple passage of the product through two dry ice traps reproducibly gave pure PF_3. The $^{31}P\{^1H\}$ NMR spectrum of a sample in $CDCl_3$ contained only PF_3 (δ 103.9); PBr_3 resonates at δ 229 while $PFBr_2$ and PF_2Br resonate at δ255 and δ195 respectively.[23] The gas phase infrared spectrum of the product was free of impurities.[24]

Scheme 1

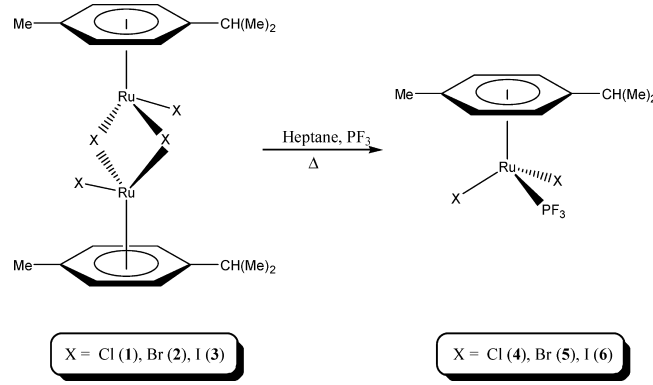

Reaction of heptane suspensions of the dimeric compounds $[RuX_2(\eta^6\text{-cymene})]_2$ (**1**)−(**3**) with PF_3 gas in Rotaflo ampoules at 70 °C for 4 to 6 h gave high yields of the products $[RuX_2(\eta^6\text{-cymene})(PF_3)]$ (**4**)−(**6**) (Scheme 1). The microcrystalline solids are bright red, red-purple, and purple, respectively, the color deepening as the halogen atomic number increases. All of the compounds (**1**)−(**6**) show the expected resonances for the cymene ligand in both their ^1H and $^{13}C\{^1H\}$ NMR spectra, consistent with rapid ring rotation about the metal center. The $^{31}P\{^1H\}$ NMR spectra of (**4**)−(**6**) contained a binomial quartet arising from coupling to the three fluorine ligands while the $^{19}F\{^1H\}$ NMR spectra consisted of a doublet in each case (see Table 1.). The corresponding spectra were run for PF_3 gas dissolved in $CDCl_3$; the values obtained were $\delta(^{31}P)$ 103.9 and $\delta(^{19}F)$ −33.49 with $J(^{31}P-^{19}F)$ −1402.7 Hz. The earliest literature values were determined many years ago with a permanent magnet system using a fixed frequency and field sweep modulation with output to an oscilloscope; the resonance frequencies corresponded to 10.97 MHz (^{31}P) and 25.49 MHz (^{19}F). Gutowsky, McCall, and Slichter obtained values of $\delta(^{31}P)$ 97.0 and $\delta(^{19}F)$ −33.6 with $J(^{31}P-^{19}F)$ −1416 Hz for liquid PF_3 with this equipment.[25] The general sign of $^1J(^{31}P-^{19}F)$ has been shown to be negative from analysis of second order spectra,[26] spin tickling,[27,28] and from the

(9) Clark, R. J.; Belefant, H.; Williamson, S. M. *Inorg. Synth.* **1989**, *26*, 12–17.
(10) Brauer, G. *Handbook of Preparative Inorganic Chemistry*, 2nd ed.; Academic Press: New York, 1963; Vol. *1*, pp 189−190.
(11) Wilkinson, G. *Nature* **1951**, *168*, 514–514.
(12) Schutzenberger, P.; Fontaine, R. *Bull. Soc. Chim.* **1872**, *17*, 482–496.
(13) Chatt, J. *Nature* **1950**, *165*, 637–638.
(14) Irvine, J. W.; Wilkinson, G. *Science* **1951**, *113*, 742–743.
(15) Wilkinson, G. *J. Am. Chem. Soc.* **1951**, *73*, 5501–5502.
(16) Rycroft, D. S.; Sharp, D. W. A.; Wright, J. G. *Inorg. Nucl. Chem. Letters* **1978**, *14*, 451–455.
(17) Davies, M. S.; Aroney, M. J.; Buys, I. E.; Hambley, T. W.; Calvert, J. L. *Inorg. Chem.* **1995**, *34*, 330–336.
(18) Frenking, G.; Wichmann, K.; Frohlich, N.; Grobe, J.; Golla, W.; Le Van, D.; Krebs, B.; Lage, M. *Organometallics* **2002**, *21*, 2921–2930.
(19) Hodson, E.; Simpson, S. J. *Polyhedron* **2004**, *23*, 2695–2707.
(20) Booth, H. S.; Bozarth, A. R. *J. Am. Chem. Soc.* **1939**, *61*, 2927–2934.
(21) Hoffman, C. J. *Inorg. Synth.* **1953**, *4*, 149–150.
(22) Williams, A. A. *Inorg. Synth.* **1957**, *5*, 95–97.
(23) Muller, A.; Niecke, E.; Glemser, O. *Z. Anorg. Allg. Chem.* **1967**, *350*, 256.
(24) Wilson, M. K.; Polo, S. R. *J. Chem. Phys.* **1952**, *20*, 1716–1719.
(25) Gutowsky, H. S.; McCall, D. W.; Slichter, C. P. *J. Chem. Phys.* **1953**, *21*, 279–292.
(26) Crocker, C.; Goodfellow, R. J. *J. Chem. Res. (M)* **1981**, 742–775.
(27) Cowley, A. H.; White, W. D.; Manatt, S. L. *J. Am. Chem. Soc.* **1967**, *89*, 6433–6437.
(28) Manatt, S. L.; Elleman, D. D.; Cowley, A. H.; Burg, A. B. *J. Am. Chem. Soc.* **1967**, *89*, 4544–4545.

Table 1. ^{19}F and ^{31}P Chemical Shifts in $CDCl_3$ Solution at 296 K

		$\delta(^{19}F)$	$\delta(^{31}P)$	$^1J(PF)$ Hz
PF_3		−33.5	103.9	−1403
$[RuCl_2(\eta^6\text{-cymene})(PF_3)]$	(**4**)	−25.4	107.6	−1370
$[RuBr_2(\eta^6\text{-cymene})(PF_3)]$	(**5**)	−21.0	107.8	−1346
$[RuI_2(\eta^6\text{-cymene})(PF_3)]$	(**6**)	−11.9	113.3	−1309
$PF_2(NMe_2)$		−65.9	141.9	−1196
$[RuCl_2(\eta^6\text{-cymene})(PF_2(NMe_2))]$	(**7**)	−44.6	137.2	−1177
$[RuBr_2(\eta^6\text{-cymene})(PF_2(NMe_2))]$	(**8**)	−43.3	136.7	−1167
$[RuI_2(\eta^6\text{-cymene})(PF_2(NMe_2))]$	(**9**)	−36.1	141.4	−1146
PCl_3			219.0	
$[RuCl_2(\eta^6\text{-cymene})(PCl_3)]$	(**10**)		141.8	
$[RuBr_2(\eta^6\text{-cymene})(PCl_3)]$	(**11**)		126.4	
$[RuI_2(\eta^6\text{-cymene})(PCl_3)]$	(**12**)		107.0	
PBr_3			229.0	
$[RuBr_2(\eta^6\text{-cymene})(PBr_3)]$	(**13**)		69.9	
$P(NMe_2)_3$			118.6	
$[RuCl_2(\eta^6\text{-cymene})(P(NMe_2)_3)]$	(**14**)		108.7	
$[RuBr_2(\eta^6\text{-cymene})(P(NMe_2)_3)]$	(**15**)		108.4	
$[RuI_2(\eta^6\text{-cymene})(P(NMe_2)_3)]$	(**16**)		109.5	

analysis of differential line broadening in solution spectra of the PFO_3^{2-} ion.[29]

Treatment of the dimers (**1**)−(**3**) with difluoro(dimethylamino)phosphine, $PF_2(NMe_2)$, in hot heptane produced the products $[RuX_2(\eta^6\text{-cymene})(PF_2(NMe_2))]$ (**7**)−(**9**) by a bridge splitting reaction (Scheme 2). The ^1H and $^{13}C\{^1H\}$ NMR spectra are again consistent with free rotation about the ruthenium−ring axis and ruthenium−phosphorus bond for each compound. In common with the trifluorophosphine compounds (**4**)−(**6**) there was no observable coupling between the fluorine atoms and the cymene ring in either the ^1H or $^{13}C\{^1H\}$ NMR spectra of (**7**)−(**9**). All of the cymene ring carbon atoms were coupled to phosphorus in the $^{13}C\{^1H\}$ NMR spectra of (**5**)−(**9**); this is unusual in that normally only the methine carbon atoms show a measurable coupling and this was indeed the case for (**4**). The $^{31}P\{^1H\}$ and $^{19}F\{^1H\}$ NMR spectra of (**7**)−(**9**) each consist of a binomial triplet and a doublet respectively and are listed in Table 1.

The lowering of the value of $^1J(^{31}P-^{19}F)$ on progression from the free ligand through (**4**) to (**6**) and through (**7**) to (**9**) is interesting. A possible explanation is that it is a consequence of the reduction of the phosphorus−fluorine bond order. The π- bonding component in the PF_3 ligand has antibonding (σ^*) P−F character and is predominantly P(3p) in nature;[30] the ligand is an exceptionally good π-acceptor,[31] and as the halide ligand on ruthenium becomes less electronegative the π-donation toward the metal center and the phosphine increases. There are unfortunately no other complete series of related compounds available for comparison, but we note that for *cis*-$[PtCl_2(PF_3)_2]$ and *cis*-$[PtBr_2(PF_3)_2]$ the values of $^1J(^{31}P-^{19}F)$ are 1326 and 1331 Hz, respectively, and for *cis*-$[RhCl(PF_3)_2]_2$ and *cis*-$[RhBr(PF_3)_2]_2$ they are 1329 and 1333 Hz, respectively.[26]

(29) Farrar, T. C.; Quintero-Arcaya, R. A. *J. Phys. Chem.* **1987**, *91*, 3224–3228.
(30) Xiao, S. X.; Trogler, W. C.; Ellis, D. E.; Berkovitch-Yellin, Z. *J. Am. Chem. Soc.* **1983**, *105*, 7033–7037.
(31) Jaw, H. R.; Zink, J. I. *Inorg. Chem.* **1988**, *27*, 3421–3424.

Scheme 2

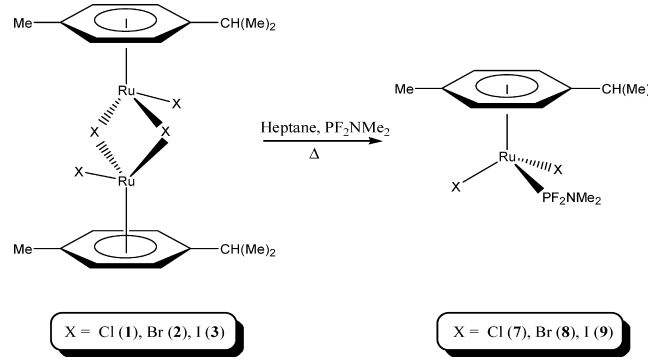

Scheme 3

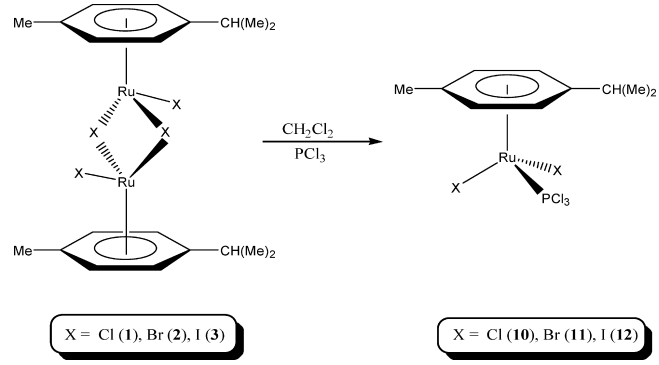

Scheme 4

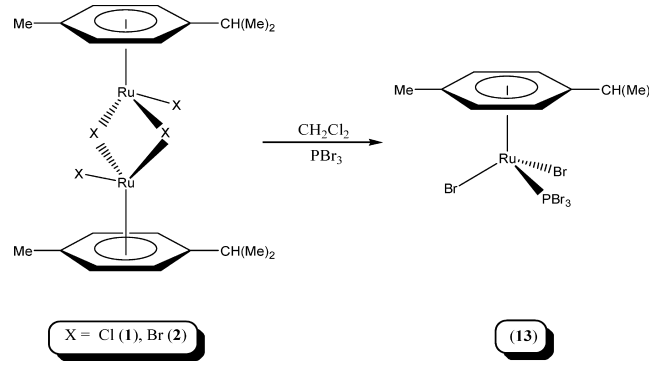

These small incremental differences and reversal of our observed trend coupled with the knowledge that the absolute sign of $^1J(^{31}P-^{19}F)$ is negative[26−29] means that subtle electronic factors may be operating, and we examine these in more detail in the computational section (vide infra).

Complexes of PCl_3 and PBr_3. The reaction of the dimers (**1**)−(**3**) with phosphorus trichloride in hot heptane was investigated and in each case led to impure products $[RuX_2(\eta^6\text{-cymene})(PCl_3)]$ contaminated with starting material and other organometallic materials. Stirring the reactants overnight in dichloromethane permitted the isolation of reasonably pure products which could be further purified by careful recrystallization (Scheme 3). The red materials (**10**)−(**12**) could be handled in dry air for short periods with stability increasing with increasing molecular weight. The compound $[RuBr_2(\eta^6\text{-cymene})(PBr_3)]$ (**13**) was prepared similarly from (**2**) and phosphorus tribromide (Scheme 4).

The reaction of the chloro dimer (**1**) with a small excess of phosphorus tribromide in heptane was carried out. The impure product which was insoluble in heptane as was the dimer (**1**) was investigated by ^{1}H and $^{31}P\{^{1}H\}$ NMR spectroscopy. The presence of four products was indicated; signals at δ69.9, 89.4, 108.2, and 126.4 were found in the $^{31}P\{^{1}H\}$ NMR spectrum. The first of these signals corresponds to (**13**) and the last corresponds to (**11**).

It is clear that halogen exchange has taken place at both the ruthenium and phosphorus centers. The two other signals could in principle belong to [RuBr(Cl)(η^6-cymene)(PBr_3)] and [RuBr(Cl)(η^6-cymene)(PCl_3)] but the resonance for the latter should lie between δ127 and δ140, the values for (**10**) and (**11**). We tentatively assign the resonance at δ89.4 to [$RuBr_2$(η^6-cymene)(PBr_2Cl)] and the resonance at δ108.2 to [$RuBr_2$(η^6-cymene)($PBrCl_2$)] because the incremental shift difference fits best for the mixed halophosphine series of dibromoruthenium compounds. The dispersion of the 400 MHz ^{1}H NMR spectrum of the mixed product did not permit us to confirm that the mixed halide at ruthenium products were not produced; these should contain diastereotopic methyl signals in the ring isopropyl substituent and four chemical shifts for the ring protons of the cymene ligand. Preliminary experiments with phosphorus triiodide indicate that (**1**), (**2**), and (**3**) are converted to [RuI_2(η^6-cymene)(PI_3)] as the sole product, the insolubility of this material both explaining the drive to a single product and hampering a full characterization. We have a displacement series where a heavy PX_3 ligand can displace a lighter halogen from a ruthenium center. The free ligands PCl_3 and PBr_3 conproportionate rapidly on mixing, and a mixture of the dimers (**1**) and (**2**) also rapidly scrambles halogen ligands in chloroform or dichloromethane solution. The mean bond energies for PF_3, PCl_3, and PBr_3 are 499.6, 318.8, and 258.2 kJ mol^{-1}, respectively. Determination of the relative bond energies in ruthenium−chloride and ruthenium−bromide systems suggests approximate values of 338 and 256 kJ mol^{-1}. These values were determined in cyclopentadienylruthenium systems[32,33] but are likely to be reasonable estimates for the cymeneruthenium case. Redistribution molar enthalpies for conproportionation should be zero if bond enthalpies were constant and transferable; generally substituted phosphines are favored over symmetrical phosphines reflecting that these bond enthalpies do not behave in that fashion.[34] The use of excess trihalophosphines in these reactions for synthetic purposes drives the exchanges toward completion and does not allow speculation on the thermodynamic driving forces behind the exchange reactions.

Scheme 5 illustrates a possible mechanism involving dissociation of the dimer into two 16 electron fragments (**A**). The PBr_3 ligand can bind via phosphorus as normal (**B**) or could ligate via bromine (**D**) and exchange halogens via bridged intermediates (**D**, **E**). The metallophosphorane (C)

Scheme 5

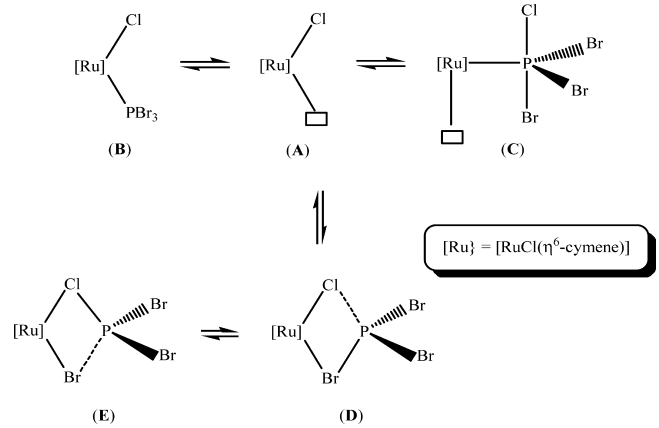

which is the formal insertion product of PBr_3 into the Ru−Cl bond is also a possible intermediate which could scramble the halogens by a turnstile process followed by de-insertion. Bending modes in (**C**) could also lead to intermediates resembling (**D**) and (**E**). We slightly favor the direct (**A**), (**D**), and (**E**) route on the grounds that it most closely resembles the situation that pertains for the fast halide scrambling between (**1**) and (**2**).

Various mechanisms for halogen exchange in free chlorophosphines have been analyzed and the concept of the phosphorus atom in such compounds having both nucleophilic and electrophilic character (biphilicity) was proposed.[35] The facile halide exchange reaction between {[Ru(η^6-C_6H_6)]$_2$(μ-Br)$_3$}BF_4 and {[Ru(η^6-C_6H_6)]$_2$(μ-Cl)$_3$}BF_4 has been reported and a tetranuclear intermediate was postulated.[36] It is clear that in this cationic case, in neutral dimer−dimer halide mixing, and the ruthenium−phosphorus halide mixing above, there are likely to be common mechanistic elements.

When the reaction of (**1**) with excess PBr_3 was repeated in dichloromethane solvent the only isolated product was (**13**) corresponding to full halogen exchange at ruthenium and reflecting that all reactants and products were soluble throughout the reaction. All of the reactions of the dimers (**1**)−(**3**) with PCl_3 or PBr_3 could be followed in situ by $^{31}P\{^{1}H\}$ NMR spectroscopy in deuterochloroform; in particular the addition of PCl_3 to (**1**) followed by subsequent addition of PBr_3 to the sample supported the dynamic situation suggested in Scheme 5.

Reaction of dichloromethane or chloroform solutions of (**10**)−(**13**) with ethanol or methanol rapidly and cleanly produced the phosphite complexes [RuX_2(η^6-cymene)-(P{OEt}$_3$)] and [RuX_2(η^6-cymene)(P(OMe)$_3$)] in isolated yields of about 60%.[19] The trifluorophosphine compounds (**4**)−(**6**) were unreactive under similar conditions. We tentatively suggest that these reactions probably proceed by nucleophilic attack on the bound trihalophosphine ligand rather than ligand dissociation followed by alcoholysis of the free PX_3 ligand and recoordination.

(32) Freeman, S. T. N.; Lemke, F. R.; Haar, C. M.; Nolan, S. P.; Petersen, J. L. *Organometallics* **2000**, *19*, 4828–4833.
(33) Luo, L.; Li, C. B.; Cucullu, M. E.; Nolan, S. P. *Organometallics* **1995**, *14*, 1333–1338.
(34) Al-Maydama, H. M. A.; Finch, A.; Gardner, P. J.; Head, A. J. *J. Chem. Thermodyn.* **1995**, *27*, 273–279.
(35) Humbel, S.; Bertrand, C.; Darcel, C.; Bauduin, C.; Juge, S. *Inorg. Chem.* **2003**, *42*, 420–427.
(36) Arthur, T.; Stephenson, T. A. *J. Organomet. Chem.* **1981**, *208*, 369–387.

Scheme 6

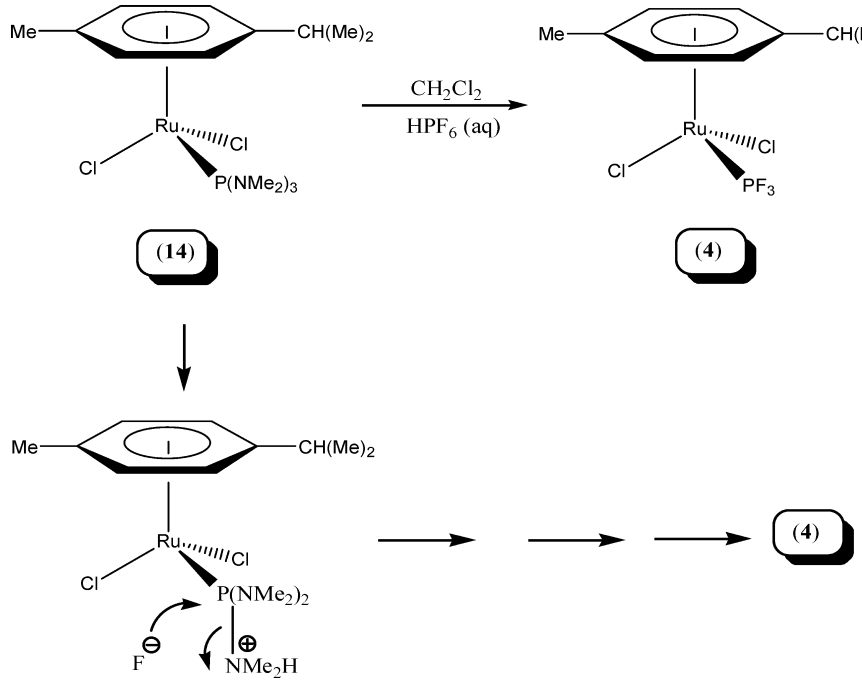

Preparation and Reactivity of $P(NMe_2)_3$ Complexes. Tris(dimethylamino)phosphine was reacted with the dimers (**1**)−(**3**) overnight in dichloromethane solution. Careful crystallization lead to the isolation of the dark red products $[RuX_2(\eta^6\text{-cymene})(P\{NMe_2\}_3)]$ (**14**)−(**16**). Our initial interest in these compounds was to investigate whether one or more of the nitrogen atoms could be induced to bind to a second metal center. The X-ray single crystal structure of tris(dimethylamino)phosphine shows that two nitrogen centers are planar and sp^2 hybridized and the third is pyramidal sp^3 hybridized.[37] There is considerable rationalization that the nitrogen lone pairs are not usually stereochemically active, and structural studies often show that the geometry at nitrogen is planar in low valent metal compounds of this ligand. We began by trying to protonate (**14**) with aqueous hexafluorophosphoric acid in dichloromethane−diethylether to ascertain if one or more of the nitrogen centers was basic. The sole isolated metal product was $[RuCl_2(\eta^6\text{-cymene})(PF_3)]$ (**4**) in 60% yield (Scheme 6). Reaction of tris(dimethylamino)-phosphine with aqueous hexafluorophosphoric acid also produces gaseous phosphorus trifluoride, and it is likely that the reaction of (**14**) to yield (**4**) does not involve the ruthenium center but is a nucleophilic attack assisted by protonation at nitrogen to provide a good leaving group.[38]

While the cleavage of P−N single bonds by haloacids is well documented the generation of a P−F bond in this manner has not been reported.[39,40] The reaction of $[Cr(CO)_5(P\{NEt_2\}_3)]$ with trimethyloxonium tetrafluoroborate produces $[Cr(CO)_5(PF\{NEt_2\}_2)]$ and only monofluorination is observed.[41] A related conversion of $[Fe(CO)_4(PF_2NEt_2)]$ to $[Fe(CO)_4(PF_2Cl)]$ using hydrogen chloride gas and of PF_2NMe_2 to PF_2X using anhydrous HX (X = Cl, Br, I) has been reported.[42,43] Kemmitt et al. have also investigated the protonolysis of a number of metal complexes of dialkylaminophosphine ligands.[44] It appears that the nitrogen center in such ligands is sufficiently basic toward strong acids despite the delocalization of the lone pair and resultant planarity at nitrogen.

Computational Analysis of the $^1J(P-F)$ Trends in Complexes (4)−(6). The observed trends for $^1J(^{31}P-^{19}F)$ upon substitution of the halide ligands might be caused by a number of effects. Examples are direct electronic effects from the halide ligands on the P−F bonds which we might further subdivide into "chemical" influences (different electronegativities, electron donor/acceptor strengths, etc.) and relativistic effects caused by spin−orbit coupling. Because the changes in the coupling constants are small compared to their magnitude, we cannot a priori rule out that the trend is caused by the increasingly strong spin−orbit coupling from Cl to Br to I and its effect on the magnetic properties of the complexes.[45] Further, the halide ligands might cause changes in the P−F coupling constants indirectly via small differences in the geometries. The most complicated scenario would be if all these effects contribute to the trend with approximately equal magnitude.

To investigate the magnitude of some of the aforementioned possible influences on $^1J(P-F)$ we have performed calculations for the $[RuX_2(\eta^6\text{-cymene})(PF_3)]$, X = Cl, Br, I

(37) Mitzel, N. W.; Smart, B. A.; Dreihaupl, K. H.; Ranin, D. W. H.; Schmidbaur, H. *J. Am. Chem. Soc.* **1996**, *118*, 12673–12682.
(38) Febvay, J.; Casabianca, F.; Riess, J. G. *J. Am. Chem. Soc.* **1984**, *106*, 7985–7986.
(39) Montemayor, R. G.; Parry, R. W. *Inorg. Chem.* **1973**, *12*, 2482–2484.
(40) Kraihanzel, C. S. *J. Organomet. Chem.* **1974**, *73*, 137–185.
(41) Hofler, M.; Stubenrauch, M.; Richarz, E. *Organometallics* **1987**, *6*, 198–199.
(42) Douglas, W. M.; Ruff, J. K. *J. Chem. Soc. A.* **1971**, 3558–3561.
(43) Bauer, D. P.; Douglas, W. M.; Ruff, J. K. *Inorg. Synth.* **1976**, *16*, 63–68.
(44) Dyer, P. W.; Fawcett, J.; Hanton, M. J.; Kemmitt, R. D. W.; Padda, R.; Singh, N. *J. Chem. Soc., Dalton Trans.* **2003**, *10*, 4–113.
(45) Autschbach, J.; Ziegler, T. *J. Chem. Phys.* **2000**, *113*, 9410–9418.

Table 2. Experimental and Calculated P−F Spin-Spin Coupling Constants $^1J(^{31}P\text{-}^{19}F)$ for $[RuX_2(\eta^6\text{-cymene})(PF_3)]$, X = Cl, Br, and I (in hertz)

complexes		ZSO/BP[e]	ZSC/BP[f]	ECP/B3LYP[g]	expt.
$[RuCl_2(\eta^6\text{-cymene})(PF_3)]$	(*a*)	−1540	−1552	−1608	−1370
	(*b*)	−1556	−1567	−1625	
	(*c*)	−1536	−1548	−1604	
$[RuBr_2(\eta^6\text{-cymene})(PF_3)]$	(*a*)	−1507	−1520	−1578	−1346
	(*b*)	−1522	−1534	−1593	
	(*c*)	−1507	−1520	−1578	
	(*d*)	−1450	−1460	−1521	
$[RuI_2(\eta^6\text{-cymene})(PF_3)]$	(*a*)	−1466	−1482	−1541	−1309
	(*b*)	−1480	−1493	−1554	
	(*c*)	−1470	−1485	−1546	
PF_3	(*a*)	−1419	−1419	−1593	−1403
	(*b*)	−1496	−1502	−1628	

[a] Optimized geometries, i.e. ZSO/BP/TZP//ZSC/BP/TZP, ZSC/BP/TZP//ZSC/BP/TZP, and ECP/B3LYP//ZSC/BP/TZP, respectively. [b] Same as (a) but geometries obtained with the QZ4P basis for Ru, P, and F; TZP for the other atoms. *J*-couplings calculated at the ZORA level (ZSO, ZSC) also based on this basis set. [c] Same as (a) but with fixed P−F bond length taken from optimized structure of Br complex. [d] Same as (c) but based on experimental structure of Br complex. [e] Relativistic ZORA spin−orbit calculation, BP functional, Slater-type basis. [f] Spin-free (scalar) ZORA calculation, BP functional, Slater-type basis. [g] B3LYP hybrid functional, scalar relativistic ECP for Ru, Gaussian-type basis.

series. Details of the computational procedure are provided in the Computational Details section. Geometry optimizations with the "BP" generalized gradient approximation (GGA) functional (at the scalar ZORA (ZSC) level) yielded average P−F bond lengths of 1.612, 1.592, 1.594, and 1.596 Å for PF_3, $[RuCl_2(\eta^6\text{-cymene})(PF_3)]$, $[RuBr_2(\eta^6\text{-cymene})(PF_3)]$, and $[RuI_2(\eta^6\text{-cymene})(PF_3)]$, respectively. The P−F bond length is very slightly increasing from chloride to the iodide complex and shorter than the P−F equilibrium bond distance calculated for PF_3 in the gas phase. Compared to experimental bond lengths of 1.569 and 1.509 Å for PF_3 and the Br complex the computations overestimate the bond distances somewhat which is an expected outcome with this type of density functional.[46] Using the Vosko−Wilk−Nusair local density approximation (LDA) functional,[47] the bond lengths are 1.590, 1.569, 1.571, and 1.573 Å, respectively, which agree better with experiment but are still somewhat too large. We have confirmed that the trend for the calculated spin−spin coupling constants does not change when geometries optimized with the LDA functional are employed instead. Results reported below are therefore based on geometries obtained with the BP functional in consistency with most of the NMR computations. The computed values of ^1J(P−F) are listed in Table 2. The trend obtained for the calculated coupling constants for the Ru complexes has the same sign and roughly the same magnitude as seen experimentally. Overall, the agreement with experiment is reasonable. The hybrid functional (B3LYP) calculations yield larger magnitudes for ^1J(P−F) than the ZSC and ZSO calculations with the non-hybrid BP functional. The couplings calculated with the TZP basis at the ZORA spin−orbit (ZSO) level are closest to the experiment, with remaining differences of 170, 161, and 157 Hz for the Cl, Br, and I complex, respectively. The deviation from experimental data is 11% in each case and within the expected error bars of the theoretical method.[48]

Using the much larger QZ4P basis for the Ru, P, and F atoms yields similar results although the agreement with experiment is slightly worse. We have observed this also in other calculations of the NMR parameters of Ru complexes[49] as well as Pt and Hg complexes.[50,51] and found recently that the use of the TZP basis seems to compensate to some extent for neglecting unspecific solvent effects.[50] (i.e., this basis provides a somewhat more balanced cancelation of errors).

For PF_3, the calculated coupling constant is smaller in magnitude than for the complexes when using a non-hybrid functional (ZSC, ZSO), and similar to the coupling in the Cl complex when using a hybrid functional (B3LYP). Experimentally, the P−F coupling in PF_3 is larger in magnitude than for the complexes. However, the experimental PF_3 value is obtained from a solution in $CDCl_3$ whereas the calculation is for the gas phase. We have also performed calculations using a continuum solvent model which, however, did not change the results significantly. For the complexes, a uniform increase of ^1J(P−F) of 7 Hz was obtained. The excellent agreement between theory and experiment for some of the calculations on PF_3 is therefore partially due to error compensation. A modeling of PF_3 in solution, as well as the dynamic solvation of the complexes, is beyond the scope of this work. It should be pointed out that while it is challenging to obtain significantly smaller error bars for the computation of *J*-couplings in metal complexes, the trends for ^1J(P−F) among these very similar complexes are correctly reproduced. Since the results are well within the deviations between density-functional theory (DFT) and experiment typically found for computations of *J*-coupling in metal complexes,[48] meaningful answers can be obtained from an analysis of the data in Table 2.

The first question that we seek to answer is whether spin−orbit coupling, a relativistic effect that increases with the nuclear charge of the halide ligand,[52,53] might be responsible for the observed trend for ^1J(P−F). A comparison of the scalar (ZSC) and the spin−orbit (ZSO) relativistic data in Table 2 shows that this is not the case. Although the trend for ^1J(P−F) due to spin−orbit effects has the right sign, it is roughly an order of magnitude smaller than what is observed experimentally. The overall magnitude of the spin−orbit contributions to the P−F coupling constants is only about 1% and for the most part originating from the Ru atom.

Regarding the mechanisms of *J*-coupling other than spin−orbit terms, it was found that contributions from the

(46) Koch, W.; Holthausen, M. C. *A Chemist's Guide to Density Functional Theory*;Wiley-VCH: Weinheim, 2001.
(47) Vosko, S. H.; Wilk, L.; Nusair, M. *Can. J. Phys.* **1980**, *58*, 1200–1211.
(48) Autschbach, J. The calculation of NMR parameters in transition metal complexes. In *Principles and Applications of Density Functional Theory in Inorganic Chemistry I*; Kaltsoyannis, N., McGrady, J. E., Eds.; Springer: Heidelberg, 2004; Vol. *112*, pp 1−48.
(49) Autschbach, J.; Zheng, S. *Magn. Reson. Chem.* **2006**, *44*, 989–1007.
(50) Sterzel, M.; Autschbach, J. *Inorg. Chem.* **2006**, *45*, 3316–3324.
(51) Jokisaari, J.; Jarvinen, S.; Autschbach, J.; Ziegler, T. *J. Phys. Chem. A.* **2002**, *106*, 9313–9318.
(52) Pyykko, P. *Chem. Rev.* **1988**, *88*, 563–594.
(53) Autschbach, J.; Ziegler, T., Relativistic Computation of NMR shieldings and Spin-spin Coupling Constants. In *Encyclopedia of Nuclear Magnetic Resonance*; Grant, D. M., Harris, R. K., Eds.; John Wiley & Sons: Chichester, 2002; Vol. *9*, pp 306−323.

relativistic analog[53,54] of the Fermi contact term (FC) differed by 25 Hz between the Cl and the Br, and by 30 Hz between the Br and the I complex, respectively, at the ZSC level. These differences are of similar magnitude as the experimental differences of 24 and 37 Hz. A more detailed analysis can therefore focus on the isotropic FC term only.

Next we investigate indirect structural effects. To this end, we have performed calculations of ^1J(P−F) for model systems where the P−F distances in the Cl and I complexes have been set to the same values as those of the optimized Br complex. The difference in the calculated ^1J(P−F) between the Cl and Br complex was 29 Hz, and between the Br and I complex it was 37 Hz (ZSO level). With the fully optimized structures for the chloride and iodide complex we obtained 33 and 41 Hz instead (Table 2). The differences in ^1J(P−F) (29/37 Hz for the fixed geometries versus 33/41 Hz for the fully optimized systems) are similar. This shows that indirect structural factors are not the main reason for the trend in ^1J(P−F) since their contributions are of the same magnitude as the spin−orbit effects and therefore significantly smaller than the total changes in ^1J(P−F). Therefore, we conclude that direct electronic effects other than spin−orbit coupling are the main reason for the observed trend. For such effects to be strong even when the moieties are separated by several chemical bonds, one might suspect that the complexes have a somewhat delocalized electronic structure. This expectation has been confirmed by our calculations, as will be discussed below in the context of the natural localized molecular orbital-natural bond order (NLMO/NBO) analysis of the P−F coupling (see Computational Details).

Spin−spin coupling constants can be analyzed using molecular orbital (MO) theory.[55] For instance, according to eq 2 from the Computational Details section, we can identify contributions to ^1J(P−F) from individual occupied MOs. The fact that Kohn−Sham DFT is based on molecular orbitals is particularly useful in this context since it allows to perform such analyses on first-principles theoretical results that are in good agreement with experiment.

For reasons stated above, the analysis focused on the isotropic FC term only. According to our calculations the main contributing orbitals are numbers 58, 76, and 92 for the Cl, Br, and I complexes, respectively, shown in Figure 1. (The different orbital numbering in the three complexes is due to the different number of core shells at the halides.) The contributions to ^1J(P−F) from these orbitals are −1572, −1558, and −1512 Hz, respectively. As is typical for MO decompositions of spin−spin coupling constants[55] there is an accompanying large contribution of opposite sign. Here, the P−F centered orbitals numbers 57, 65, and 83 contribute +573, +564, and +559 Hz in the Cl, Br, and I complexes, respectively. The two sets of orbitals which were identified here as the biggest contributors to ^1J(P−F) are qualitatively the same as those calculated for free PF_3. The sign of the trend for the sum, as well as for the largest individual MO contributions, is the same as in the experiment, but the trend is strongly overestimated and there are a large number of additional MOs contributing to ^1J(P−F) with varying signs. These contributions add up to several hundred hertz. It was not possible to identify a single or a few MOs that would yield most of the observed trend. From the MO analysis it appears that the trend ^1J(P−F) in the complexes is in part caused by a small perturbation of the PF_3 orbitals and by a large number of small but significant contributions from other MOs which are mainly centered on the metal and the other ligands but have small amplitudes on the PF_3 moiety. These findings are in line with the statement made above about "subtle electronic effects". We interpret this situation as the complexes possessing a somewhat delocalized electronic structure in which the halide ligands can have electronic influence on the P−F bonds and therefore affect the P−F coupling constant. The subtlety of these effects is highlighted by the fact that a "fragment orbital" analysis[56] performed by us did not find any significant *direct* contributions from the halide atomic orbitals to ^1J(P−F).

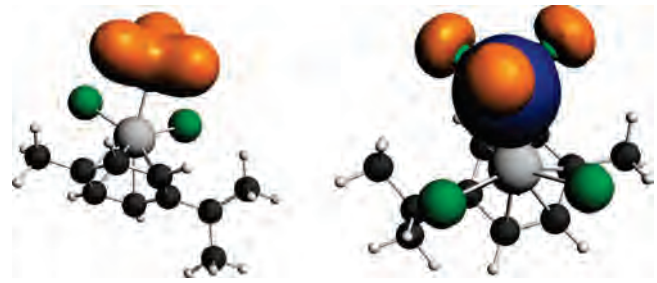

Figure 1. P−F bonding occupied molecular orbitals with large phosphorus σ-bond character in [$RuX_2(\eta^6$-cymene)(PF_3)], X = Cl, Br, and I. Shown here are orbitals # 65 (left) and 76 (right) for the Br complex. The equivalent orbitals for the Cl (# 47, 58) and I (# 83, 92) complex are visually indistinguishable from this orbital and therefore not shown.

To support the conclusions from the MO analysis we have developed a program for the analysis of spin−spin coupling constants obtained from relativistic DFT computations using "natural" localized molecular orbitals (NLMOs) and natural bond orbitals (NBOs) as described in the Computational Details section. The analysis closely follows the "natural" shielding and spin−spin coupling analyses proposed by Bohmann et al.[57] and decomposes the *J*-coupling into terms from perfectly localized Lewis-type (L) bond and lone-pair orbitals ("natural bond orbitals" or NBOs) and additional delocalized non-Lewis (NL) terms for each parent NBO. The analysis can be applied to couplings involving light, as well as heavy, nuclei. The $CHOOSE keyword was applied in the NBO computations to obtain P−F bonding and Ru−P bonding parent NBOs for the set of NLMOs used for the analysis. As with the other analyses (MO and fragment orbitals) discussed here, a considerable number of NLMOs contribute to the final result, and it was not possible to determine a single orbital or a sum of a few orbitals that would yield the exact magnitude for the trend. Some of the contributions are listed in Table 3.

The biggest contributors to ^1J(P−F) are fluorine valence lone pair orbitals with large F 2s character, the Ru−P bond,

(54) Autschbach, J.; Ziegler, T. *J. Am. Chem. Soc.* **2001**, *123*, 3341–3349.
(55) Autschbach, J.; Le Guennic, B. *Chem.—Eur. J.* **2004**, *10*, 2581–2589.
(56) Autschbach, J.; Igna, C. D.; Ziegler, T. *J. Am. Chem. Soc.* **2003**, *125*, 1028–1032.
(57) Bohmann, J. A.; Weinhold, F.; Farrar, T. C. *J. Chem. Phys.* **1997**, *107*, 1173–1184.

Table 3. Averaged Fluorine Core Orbital (C), Valence Lone Pair (LP), Ru−P, Ru−X and P−F bonding (B) NLMO Contributions to ^1J(P−F) in [$RuX_2(\eta^6$-cymene)(PF_3)], X = Cl, Br, and I (in hertz)[a]

complex/NLMO	B(Ru-X)	F(LP)	F(C)	B(P−F)	B(Ru−P)
[$RuCl_2(\eta^6$-cymene)(PF_3)]	−2	−613	−316	235	−447
[$RuBr_2(\eta^6$-cymene)(PF_3)]	4	−613	−314	234	−434
[$RuI_2(\eta^6$-cymene)(PF_3)]	−1	−603	−313	233	−415

[a] The summations of these five main contributions yield −1143, −1123, and −1099 Hz for the Cl, Br, and I complexes, respectively. These five main contributions represent the correct trend, and the summations yields approximately 70% of the total computed J(P−F).

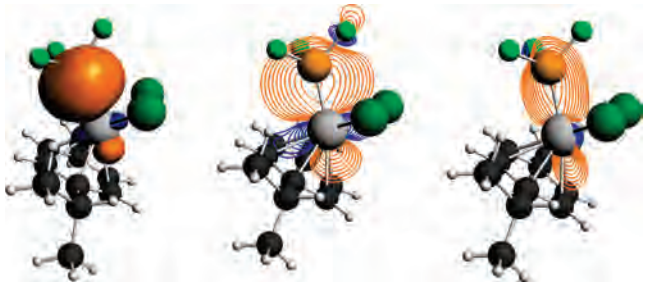

Figure 2. One of three Ru−P sigma-bonding NLMO in [$RuX_2(\eta^6$-cymene)(PF_3)]: 3D isosurface (0.03 au) and 2D contour plots in planes through Ru−P−F and X−Ru−P. Contour line values: 0.01 to 3.00. Shown here are the orbitals for the X = Br complex. The corresponding orbitals for the Cl and I complex are very similar and therefore not shown.

the fluorine 1s orbitals, and P−F bond. The first two contributions are intuitive and similar to the outcome of a fragment orbital analysis.[58,61,62] The 1s contributions are large but mostly transferable between the complexes and therefore do not need to be considered for the trend in ^1J(P−F). Ru−X bond contributions are not significant for the trend but listed for completeness.

The most interesting contributions originate from the Ru−P bond NLMOs as listed in Table 3 (NLMO #3 in each case). Visualizations of one of these orbitals are shown in Figure 2. The contributions from this NLMO yield the correct trend for ^1J(P−F) although its magnitude does not completely account for the differences in ^1J(P−F) between the Cl, Br, and I complexes. According to the NLMO analysis of the J-coupling, the non-Lewis (NL, delocalization) terms from these orbitals amount to about 15% of their total contribution to ^1J(P−F). In each case the parent Ru−P bond NBO has a small (∼ 0.4%), but obviously significant, involvement of each halide ligand which increases along the series Cl, Br, and I along with contributions from the fluorine atoms. The latter contributions are clearly visible in the contour line diagrams in Figure 2, while the halide contributions only become visible if contour lines with values below 0.01 are included. Additional information about the influence of the metal and the other ligands on the PF_3 moiety is obtained from the composition of the atomic hybrid orbitals to the NLMOs, as determined by the NBO computation. For the P−F bonding NLMOs, we find that the contributing phosphorus AO has roughly 10% s character in the computation for free PF_3 but approximately 20% s character in the complexes. There is also an increase in the phosphorus charge when going from the free ligand to the complexes, along with a slight increase in the populations of the antibonding P−F σ^* NBOs. These results highlight the considerable metal ligand back bonding capability of PF_3 which has recently been analyzed in detail (along with other ligands of the type YX_3) by Leyssens et al.[59] The participation of the P−F antibonding orbitals in the back-donation helps to rationalize the results from the NLMO analysis of ^1J(P−F).

Among the analysis tools employed here the NLMO analysis provides the clearest evidence for a direct involvement of the halide orbitals in the P−F spin−spin coupling via participation in a somewhat delocalized Ru−P bond. We attribute the small decrease in the magnitude of ^1J(P−F) along the series Cl, Br, and I to an increased delocalization of charge away from the PF_3 moiety. These effects are indeed rather subtle and highlight some of the general difficulties of analyzing trends for NMR parameters in transition metal complexes because of a complicated interplay of metal and ligand orbitals where some amount of delocalization is not uncommon.[54,56,60−62] It appears, however, that a NLMO analysis is helpful in such cases to address such questions of delocalization and to pick out the main contributing orbitals to the NMR spin−spin coupling.[62]

Crystal Structural Determinations. The single crystal X-ray structures of (**5**), (**8**), and (**16**) were determined to provide a series of related compounds containing the PF_3, $PF_2(NMe_2)$, and $P(NMe_2)_3$ ligands in a relatively sterically unhindered environment. The collection and refinement parameters are shown in Table 4, and selected bond lengths and bond angles are given in Table 5.

The interligand angle at phosphorus in gaseous PF_3 is 97.7(2)° with the P−F bond length being 1.569(1) Å;[63] the average P−F bond length in (**5**) (Figure 3) is 1.509(8) Å which is an appreciable shortening. This parameter covers the range from 1.51−1.57 Å in the reported structures in the literature with most determinations finding about 1.55Å; we repeateded our determination using a second crystal and obtained an average value of 1.508(9) Å and conclude that the bond shortening is significant. The Ru−P bond length of 2.184 Å in (**5**) compares well with 2.178 Å and 2.206(2) Å in [$RuCl_2\{\eta^2$:η^3-CH_2=C(Me)CH$(PCy_3)(CH_2)_2$CHC(Me)$CH_2\}(PF_3)$] and *trans*-[Ru(H)$(PF_3)(dppm)_2$]BF_4, respectively.[64,65]

The free ligand difluoro(dimethylamino)phosphine has been structurally characterized in the solid state, and the P−F and P−N bond lengths are 1.610(4) Å and 1.626(5) Å, respectively, with angles of 91.5(3)° and 101.6(2)° for F−P−F and F−P−N, respectively.[66] There is a small shortening of the P−F bond in (**8**) relative to the free ligand

(58) Chen, W.; Liu, F; Matsumoto, K.; Autschbach, J.; Le Guennic, B.; Ziegler, T.; Maliarik, M.; Glaser, J. *Inorg. Chem.* **2006**, *45*, 4526–4536.
(59) Leyssens, T.; Peters, D.; Orpen, A. G.; Harvey, J. N. *Organometallics* **2007**, *26*, 2637–2645.
(60) Autschbach, J.; Ziegler, T. *J. Am. Chem. Soc.* **2001**, *123*, 5320–5324.
(61) Le Guennic, B.; Matsumoto, K.; Autschbach, J. *J. Magn. Reson. Chem.* **2004**, *42*,, S99−S116.
(62) Autschbach, J.; Le Guennic, B. *J. Chem. Educ.* **2007**, *84*, 156–171.
(63) Williams, Q.; Sheridan, J.; Gordy, W. *J. Chem. Phys.* **1952**, *20*, 164–167.
(64) Nanishankar, H. V.; Nethaji, M.; Jagirdar, B. R. *Eur. J. Inorg. Chem.* **2004**, 3048–3056.

Table 4. Data Collection and Refinement Parameters for (**5**), (**8**), and (**16**)

Identification code	(**5**)	(**8**)	(**16**)
empirical formula	$C_{10}H_{14}Br_2F_3PRu$	$C_{12}H_{20}Br_2F_2NPRu$	$C_{16}H_{32}I_2N_3PRu$
formula weight	483.07	508.15	652.29
temperature	223(2) K	294(2) K	294(2) K
wavelength	0.71073 Å	0.71073 Å	0.71073 Å
crystal system	orthorhombic	monoclinic	monoclinic
space group	*Fdd*2	$P2_1/n$	$P2_1/c$
unit cell dimensions	a = 25.809(3) Å, α = 90°	a = 9.5131(5) Å, α = 90°	a = 9.6415(7) Å, α = 90°
	b = 26.015(4) Å, β = 90°	b = 11.3369(12) Å, β = 103.033(6)°	b = 15.1527(11) Å, β = 103.664(7)°
	c = 9.0051(11) Å, γ = 90°	c = 15.6280(12) Å, γ = 90°	c = 15.666(2) Å, γ = 90°
volume	6046.3(13) Å^3	1642.0(2) Å^3	2223.9(3) Å^3
Z	16	4	4
density (calculated)	2.123 Mg/m^3	2.055 Mg/m^3	1.948 Mg/m^3
absorption coefficient	6.438 mm^{-1}	5.925 mm^{-1}	3.556 mm^{-1}
F(000)	3680	984	1256
crystal size	0.35 × 0.25 × 0.25 mm^3	0.30 × 0.25 × 0.25 mm^3	0.30 × 0.25 × 0.25 mm^3
theta range for data collection	2.22 to 27.50°.	2.24 to 27.50°.	1.90 to 28.50°.
index ranges	$-33 \le h \le 1$	$-12 \le h \le 1$	$-12 \le h \le 1$
	$-1 \le k \le 33$	$-14 \le k \le 1$	$-1 \le k \le 20$
	$-1 \le l \le -11$	$-20 \le l \le 20$	$-20 \le l \le 21$
reflections collected	2242	4856	7056
independent reflections	2046 [R(int) = 0.0272]	3752 [R(int) = 0.0232]	5619 [R(int) = 0.0326]
refinement method	full-matrix least-squares on F^2	full-matrix least-squares on F^2	full-matrix least-squares on F^2
data/restraints/parameters	2046/1/154	3752/0/173	5617/0/208
goodness-of-fit on F^2	1.034	1.048	1.080
final R indices [I > 2sigma(I)]	R1 = 0.0332, wR2 = 0.0705	R1 = 0.0315, wR2 = 0.0714	R1 = 0.0366, wR2 = 0.0796
R indices (all data)	R1 = 0.0430, wR2 = 0.0747	R1 = 0.0420, wR2 = 0.0756	R1 = 0.0525, wR2 = 0.0859
largest diff. peak and hole	0.542 and −0.562 e Å^{-3}	0.559 and −0.649 e Å^{-3}	0.562 and −1.284 e Å^{-3}

Table 5. Selected Bond Lengths (Å) and Bond Angles (deg) for (**5**), (**8**), and (**16**)

	(**5**)	(**8**)	(**16**)		(**5**)	(**8**)	(**16**)
Ru(1)−P(1)	2.184(2)	2.2446(9)	2.3657(11)	Br(1)−Ru(1)−Br(2)	89.30(4)	88.16(2)	
Ru(1)−Br(1)	2.5267(11)	2.5127(5)		I(1)−Ru(1)−I(2)			90.303(14)
Ru(1)−Br(2)	2.5253(9)	2.5351(5)		Br(1)−Ru(1)−P(1)	83.85(9)	86.96(3)	
Ru(1)−I(1)			2.7416(5)	Br(2)−Ru(1)−P(1)	85.86(7)	87.08(3)	
Ru(1)−I(2)			2.7359(4)	I(1)−Ru(1)−P(1)			91.83(3)
P(1)−F(1)	1.510(10)	1.563(2)		I(2)−Ru(1)−P(1)			88.79(3)
P(1)−F(2)	1.516(6)	1.571(2)		F(1)−P(1)−F(2)	97.4(5)	94.64(15)	
P(1)−F(3)	1.502(8)			F(2)−P(1)−F(3)	97.6(5)		
P(1)−N(1)		1.612(4)	1.673(3)	F(1)−P(1)−F(3)	97.2(6)		
P(1)−N(2)			1.671(4)	F(1)−P(1)−N(1)		101.02(18)	
P(1)−N(3)			1.667(4)	F(2)−P(1)−N(1)		103.86(17)	
				N(1)−P(1)−N(2)			104.2(2)
				N(2)−P(1)−N(3)			100.3(2)
				N(1)−P(1)−N(3)			105.9(2)

which is not so pronounced as that observed in (**5**) with other ligand parameters being essentially unchanged on coordination to the ruthenium center; this determination is the first report of a platinum group metal complex of this ligand

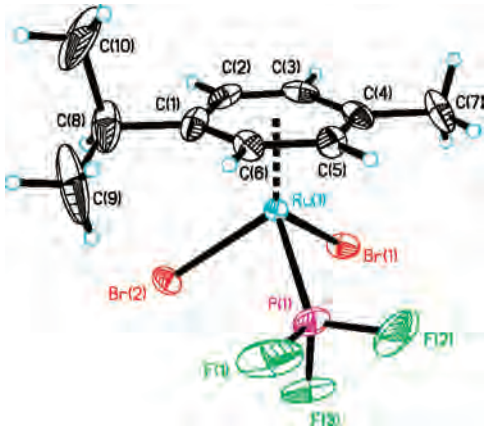

Figure 3. X-ray single crystal structure of (**5**). Thermal ellipsoids are drawn at the 50% probability level.

(Figure 4). The angle sum around N(1) is 358.9° reflecting the rehybridization of the nitrogen lone pair also observed in the free ligand.

The three angle sums at nitrogen in (**16**) are 357.3°, 359.4°, and 360.0° indicating trigonal planar geometry at all three nitrogen centers (Figure 5) in contrast to the free ligand.[37] This geometry is commonly found on coordination to a metal center[67,68] but in the iron complex $[Fe(CO)_3(P\{NMe_2\}_3)_2]$ one of the aminophosphine ligands has a geometry comparable to the free ligand. It has been suggested that the barrier to inversion at nitrogen is low for this ligand.

The Ru−P bond lengths of (**5**), (**8**), and (**16**) show a progressive lengthening associated with increasing σ-donor strength and decreasing π-donor strength of the phosphine ligands.[69]

(65) Werner, H.; Stuer, W.; Jung, S. F.; Weberndorfer, B.; Wolf, J. *Eur. J. Inorg. Chem.* **2002**, 1076–1080.
(66) Morris, E. D.; Nordman, C. E. *Inorg. Chem.* **1969**, *8*, 1673–1676.
(67) Brunet, J. J.; Diallo, O.; Donnadieu, B.; Roblou, E. *Organometallics* **2002**, *21*, 3388–3394.
(68) Wang, K.; Emge, T. J.; Goldman, A. S. *Organometallics* **1994**, *13*, 2135–2137.

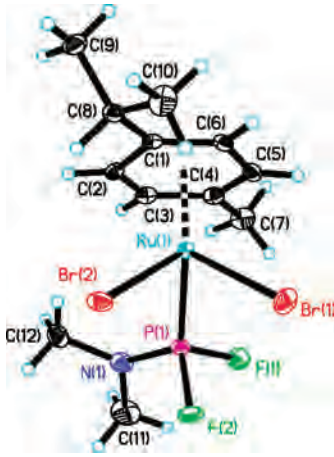

Figure 4. X-ray single crystal structure of (**8**). Thermal ellipsoids are drawn at the 50% probability level.

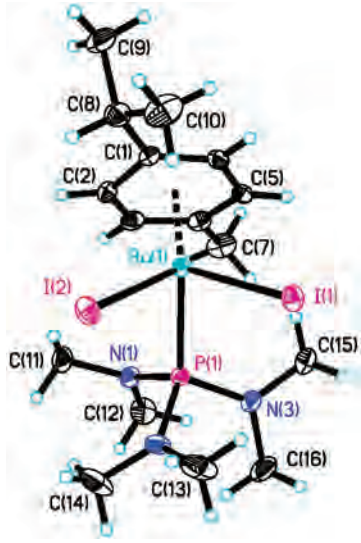

Figure 5. X-ray single crystal structure of (**16**). Thermal ellipsoids are drawn at the 50% probability level.

Conclusions

The half-sandwich cymeneruthenium moiety [$RuX_2(\eta^6$-cymene)] has been shown to provide a stable platform for the coordination of trihalophosphine ligands PF_3, PCl_3, and PBr_3. Tris(dimethylamino)phosphine complexes have also been prepared, and a small number of reactions have been carried out to investigate the reactivity of the four bound ligands. Alcoholysis of the PCl_3 and PBr_3 but not the PF_3 complexes proceeds in good yield resulting in the corresponding trialkylphosphite complexes. The conversion of the coordinated tris(dimethylamino)phosphine ligand in [$RuX_2(\eta^6$-cymene)($P\{NMe_2\}_3$)] (**14**)−(**16**) by reaction with aqueous hexafluorophosphoric acid to a coordinated trifluorophosphine ligand resulting in the isolation of [$RuX_2(\eta^6$-cymene)(PF_3)] (**4**)−(**6**) has been observed. Both of these reactions may well proceed as an example of nucleophilic attack at ligand chemistry rather than involving dissociation−association chemistry.

Reaction of the dimers [$RuX_2(\eta^6$-cymene)]$_2$ (**1**)−(**3**) with trihalophosphines led in some cases to exchange of ruthenium bound halide ligands with heavier halide ligands initially bound to phosphorus. This uncommon process in non-polar media has been explained by suggesting that the PX_3 molecule can bind to a metal center either by a conventional metal−phosphorus bond or by a halide to metal donor bond producing a four center intermediate which undergoes asymmetric bridge cleavage. The similarity of this process to the rapid halide ligand scrambling observed when, for example, (**1**) and (**2**) are mixed inclines us to slightly disfavor an alternative metallophosphorane pathway at present. Since the fluoro dimer [$RuF_2(\eta^6$-cymene)]$_2$ is unknown and has resisted our synthetic efforts, we are unable to settle this mechanistic question by well established NMR techniques, the remaining halogens being quadrupolar and therefore ruling out exchange studies and identification of intermediates using ^{31}P NMR observation. Similarly the alcoholysis and protonation reactions could involve five coordinate metallophosphorane intermediates but in these cases as in the halide scrambling reactions we favor simple pathways that most closely resemble well established organic reaction pathways. It is to be hoped that others will perform appropriate calculations to settle this point.

Study of two series of complexes [$RuX_2(\eta^6$-cymene)(PF_3)] and [$RuX_2(\eta^6$-cymene)($PF_2(NMe_2)$)] reveals a decrease in ^1J(P−F) as the halide ligand is changed from chloride through to iodide; calculation studies suggest that the electronic and orbital effects are subtle. From a computational analysis in terms of localized orbitals, the trend has been shown to originate from an involvement of the halide orbitals in a somewhat delocalized ruthenium−phosphorus bond while several other possible factors such as geometry differences among the complexes or spin−orbit coupling at the halide centers were ruled out as sources for the trends.

Experimental Section

All reactions and preparations were carried out on a vacuum/nitrogen line using standard Schlenk-tube techniques. Diethylether, hexane, heptane, and petroleum ether (40−60 °C) were dried over sodium wire and distilled under nitrogen. Dichloromethane was dried over barium oxide and distilled under nitrogen. All solvents were degassed prior to use. All products isolated were dried under reduced pressure, in a hot water bath for at least 1 h. Infrared spectra were recorded on a Bruker Vector 22 FTIR instrument; only significant absorption bands are reported. NMR spectra were recorded on Bruker Avance 300 (300.13 MHz, ^{1}H; 75.47 MHz, ^{13}C; 121.49 MHz ^{31}P) and Bruker Avance 400 (400.13 MHz, ^{1}H; 376.50 MHz ^{19}F; 100.62 MHz, ^{13}C; 161.98 MHz ^{31}P) spectrometers. All ^{1}H and ^{13}C NMR chemical shifts are expressed in ppm relative to residual protonated solvent. The high-frequency positive convention was followed for ^{19}F chemical shifts (1% C_6F_6 in $CDCl_3$ −162.60 ppm) and ^{31}P NMR chemical shifts (1% $P(OPh)_3$ in $CDCl_3$ +126.5 ppm). All NMR and infrared spectra were measured at room temperature. Standard Bruker microprograms were used for the acquisition of HETCORR, NOESY, and COSY-45 spectra. Elemental analyses were obtained at Manchester University Analytical laboratories. Fast Atom Bombardment (FAB) mass spectra were

(69) Yarbrough, L. W.; Hall, M. B. *Inorg. Chem.* **1978**, *17*, 2269–2275.

obtained on a Kratos Concept S1 spectrometer. The dimers $[RuX_2(\eta^6\text{-cymene})]_2$ (X = Cl[19], Br, I[70]) were prepared by literature methods.

Phosphorus trichloride, phosphorus tribromide, and tris(dimethylamino)phosphine were obtained from Aldrich and transferred to Rotaflo ampoules for storage under nitrogen. Dichloro(dimethylamino)phosphine was prepared by a literature method[71] and converted to difluoro(dimethylamino)phosphine by treatment with antimony trifluoride in the absence of solvent.[72,73] Trifluorophosphine (0.01−0.02 mol) was prepared by dropwise addition of PBr_3 to excess powdered SbF_3; the use of a nitrogen gas sweep, entrainment through two traps (−78 °C), and collection at −196 °C produced a pure product (^{31}P and ^{19}F NMR analysis).

Caution! *Trifluorophosphine is a very toxic gas and should be handled in a well ventilated area by experienced personnel. The scale used in the experimental section presents a minimal but finite hazard.*

Preparation of $[RuX_2(\eta^6\text{-cymene})(PF_3)]$, X = Cl (4), Br (5), I (6). The appropriate dimer compound $[RuX_2(\eta^6\text{-cymene})]_2$ (0.5−0.8 g) was suspended in heptane (30 mL) in a Rotaflo ampule (175 mL) equipped with a magnetic flea. The reactants were degassed, and the ampule was filled with nitrogen gas. The ampule was placed in a liquid nitrogen bath, and freshly prepared trifluorophosphine (0.01−0.02 mol) was swept into the ampule through a lead through adaptor where it was observed to freeze onto the walls of the ampule as a white film. The nitrogen carrier gas was removed via the sidearm of the ampule. Adjustment of the nitrogen flow rate allowed the process to be monitored by occasional pressure release at a manostat. Finally, the gas generator was rapidly detached from the ampule which was sealed with the Rotaflo barrel, degassed, and refilled with nitrogen while still at −196 °C. Cautious warming to room temperature behind a safety screen (calculated pressure is ca. 35 psi at room temperature), and stirring at 70 °C for 6−12 h produced visible color changes. The cooled suspensions were filtered, washed with pentane (2 × 20 mL), and dried under reduced pressure. Isolated yields were essentially quantitative of bright red, red-purple, and purple solids, respectively.

$[RuCl_2(\eta^6\text{-cymene})PF_3]$ (4). (Found: C, 30.34; H, 3.45%; $C_{10}H_{14}F_3Cl_2P_1Ru$ calcd: C, 30.47; H, 3.58%); ^1H NMR ($CDCl_3$): δ 1.27 (d, J(HH) 7.0 Hz, 6H, $CH(CH_3)_2$,), 2.29 (s, 3H, CH_3-ring), 2.88 (sept, J(HH) 7.0 Hz, 1H, $CH(CH_3)_2$), 5.72 (d, J(HH) 7.0 Hz, 2H, *CH*-ring), 5.85 (d, J(HH) 7.0 Hz, 2H, *CH*-ring); $^{31}P\{^1H\}$ NMR ($CDCl_3$): δ 107.4 (q, J(P−F) 1370 Hz); $^{13}C\ \{^1H\}$ NMR ($CDCl_3$): δ 112.81 (s, C1-ring), 108.78 (s, C4-ring), 91.34 (d, J(P−C) 8.0 Hz, C2,6-ring), 90.98 (d, J(P−C) 6.0 Hz, C3,5-ring), 31.17 (s, $CH(CH_3)_2$), 22.03 (s, $CH(CH_3)_2$), 18.89 (s, CH_3-ring); $^{19}F\{^1H\}$ NMR ($CDCl_3$): δ −25.4 (d, J(P−F) 1370 Hz).

$[RuBr_2(\eta^6\text{-cymene})PF_3]$ (5). (Found: C, 24.10; H, 2.89%; $C_{10}H_{14}F_3Br_2P_1Ru$ calcd: C, 24.86; H, 2.92%); ^1H NMR ($CDCl_3$): δ 1.26 (d, J(HH) 7.0 Hz, 6H, $CH(CH_3)_2$), 2.38 (d, J(PH) 1.05 Hz, 3H, CH_3-ring), 2.95 (sept, J(HH) 7.0 Hz, 1H, $CH(CH_3)_2$), 5.73 (d, J(HH) 6.5 Hz, 2H, *CH*-ring), 5.85 (d, J(HH) 6.5 Hz, 2H, *CH*-ring); $^{31}P\{^1H\}$ NMR ($CDCl_3$): δ 107.67 (q, J(P−F) 1346 Hz); $^{13}C\ \{^1H\}$ NMR ($CDCl_3$): δ 114.10 (d, J(P−C) 3.8 Hz, C1-ring), 108.97 (d, J(P−C) 3.8 Hz, C4-ring), 91.44 (d, J(P−C) 7.7 Hz, C2,6-ring), 90.93 (d, J(P−C) 5.5 Hz, C3,5-ring), 31.46 (s, $CH(CH_3)_2$), 22.16 (s, $CH(CH_3)_2$), 19.51 (s, CH_3-ring); $^{19}F\{^1H\}$ NMR ($CDCl_3$): δ −21.0 (d, J(P−F) 1346 Hz).

$[RuI_2(\eta^6\text{-cymene})PF_3]$ (6). (Found: C, 20.34; H, 2.42%; $C_{10}H_{14}F_3P_1I_2Ru$ calcd: C, 20.81; H, 2.45%); ^1H NMR ($CDCl_3$): δ 1.29 (d, J(HH) 7.0 Hz, 6H, $CH(CH_3)_2$), 2.59 (s, 3H, CH_3-ring), 3.15 (sept, J(HH) 7.0 Hz, 1H, $CH(CH_3)_2$), 5.74 (d, J(HH) 7.0 Hz, 2H, *CH*-ring), 5.89 (d, J(HH) 7.0 Hz, 2H, *CH*-ring); $^{31}P\{^1H\}$ NMR ($CDCl_3$): δ 113.3 (q, J(P−F) 1309 Hz); $^{13}C\ \{^1H\}$ NMR ($CDCl_3$): δ 116.56 (s, C1-ring), 109.32 (s, C4-ring), 91.55 (d, J(P−C) 8.0 Hz, C2,6-ring), 91.96 (d, J(P−C) 6.0 Hz C3,5-ring), 32.11 (s, $CH(CH_3)_2$), 22.61 (s, $CH(CH_3)_2$), 20.65 (s, CH_3-ring); $^{19}F\{^1H\}$ NMR ($CDCl_3$): δ −11.9 (d, J(P−F) 1309 Hz).

Preparation of $[RuX_2(\eta^6\text{-cymene})(PF_2(NMe_2))]$, X = Cl (7), Br (8), I (9). The appropriate dimer compound $[RuX_2(\eta^6\text{-cymene})]_2$ (0.5−0.8 g) was suspended in heptane (30 mL) in a Rotaflo ampule (125 mL) equipped with a magnetic flea. Difluoro(dimethylamino)phosphine (0.3 mL, excess) was added, and the reactants were degassed and saturated with nitrogen gas. Stirring at 70 °C for 6−12 h produced visible color changes. The cooled suspensions were filtered, washed with pentane (2 × 20 mL), and dried under reduced pressure. Isolated yields were essentially quantitative of bright red, red-purple, and purple solids respectively.

$[RuCl_2(\eta^6\text{-cymene})(PF_2(NMe_2))]$ (7). (Found: C, 34.18; H, 4.83; N, 3.27%; $C_{12}H_{20}F_2Cl_2N_1P_1Ru$ calcd: C, 34.38; H, 4.81; N, 3.34%); ^1H NMR ($CDCl_3$): δ 1.22 (d, J(HH) 7.0 Hz, 6H, $CH(CH_3)_2$), 2.19 (s, 3H, CH_3-ring), 2.86 (dt, J(P−H) 11 Hz, J(F−H) 3 Hz, 6H, $PF_2(NMe_2)$), 2.88 (sept, J(HH) 7.0 Hz, 1H, $CH(CH_3)_2$), 5.55 (d, J(HH) 6.1 Hz, 2H, *CH*-ring), 5.68 (d, J(HH) 6.1 Hz, 2H, *CH*-ring); $^{31}P\{^1H\}$ NMR ($CDCl_3$): δ 137.2 (t, J(P−F) 1177 Hz); $^{13}C\ \{^1H\}$ NMR ($CDCl_3$): δ 110.89 (d, J(P−C) 2 Hz, C1-ring), 104.56 (d, J(P−C) 2 Hz, C4-ring), 90.68 (d, J(P−C) 6.5 Hz, C2,6-ring), 89.68 (d, J(P−C) 5.5 Hz, C3,5-ring), 36.72 (d, J(P−C) 6.5 Hz, $PF_2(NMe_2)$), 30.64 (s, $CH(CH_3)_2$), 21.88 (s, $CH(CH_3)_2$), 18.37 (s, CH_3-ring). ^{19}F NMR ($CDCl_3$): δ −44.55 (d sept, J(P−F) 1177 Hz, J(F−H) 3 Hz).

$[RuBr_2(\eta^6\text{-cymene})(PF_2(NMe_2))]$ (8). (Found: C, 28.05; H, 4.13; N, 2.67%; $C_{12}H_{20}F_2Br_2N_1P_1Ru$ calcd: C, 28.36; H, 3.97; N, 2.76%); ^1H NMR ($CDCl_3$): δ 1.24 (d, J(HH) 7.0 Hz, 6H, $CH(CH_3)_2$), 2.32 (s, 3H, CH_3-ring), 2.88 (dt, J(P−H) 11.2 Hz, J(F−H) 2.8 Hz, 6H, $PF_2(NMe_2)$), 2.98 (sept, J(HH) 7 Hz, 1H, $CH(CH_3)_2$), 5.53 (d, J(HH) 6.0 Hz, 2H, *CH*-ring), 5.69 (d, J(HH) 6.0 Hz, 2H, *CH*-ring); $^{31}P\{^1H\}$ NMR ($CDCl_3$): δ 136.7 (t, J(P−F) 1167 Hz; $^{13}C\ \{^1H\}$ NMR ($CDCl_3$): δ 112.35 (d, J(P−C) 3.5 Hz, C1-ring), 105.58 (d, J(P−C) 3.0 Hz, C4-ring), 90.02(d, J(P−C) 6.0 Hz, C2,6-ring), 89.63 (d, J(P−C) 5.5 Hz, C3,5-ring), 37.34 (d, J(P−C) 6.5 Hz, $PF_2(NMe_2)$), 31.09 (s, $CH(CH_3)_2$), 22.14 (s, $CH(CH_3)_2$), 19.04 (s, CH_3-ring). ^{19}F NMR ($CDCl_3$): δ −43.26 (d sept, J(P−F) 1167 Hz, J(F−H) 3 Hz).

$[RuI_2(\eta^6\text{-cymene})(PF_2(NMe_2))]$ (9). (Found: C, 23.58; H, 3.03; N, 2.27%; $C_{12}H_{20}F_2I_2N_1P_1Ru$ calcd: C, 23.94; H, 3.35; N, 2.33%); ^1H NMR ($CDCl_3$): δ 1.26 (d, J(HH) 7.0 Hz, 6H, $CH(CH_3)_2$), 2.49 (d, J(P−H) 0.9 Hz, 3H, CH_3-ring), 2.89 (dt, J(P−H) 11.0 Hz, 6H, J(F−H) 2.8 Hz, $PF_2(NMe_2)$), 3.15 (sept, J(HH) 7 Hz, 1H, $CH(CH_3)_2$), 5.53 (d, J(HH) 6.0 Hz, 2H, *CH*-ring), 5.71 (d, J(HH) 6.0 Hz, 2H, *CH*-ring); $^{31}P\{^1H\}$ NMR ($CDCl_3$): δ 141.53 (t, J(P−F) 1146 Hz); $^{13}C\ \{^1H\}$ NMR ($CDCl_3$): δ 114.53 (d, J(P−C) 5.0 Hz, C1-ring), 106.87 (d, J(P−C) 4.5 Hz, C4-ring), 90.28(d, J(P−C) 5.0 Hz, C2,6-ring), 90.09 (d, J(P−C) 4.5 Hz, C3,5-ring), 38.25 (d, J(P−C) 6.5 Hz, $PF_2(NMe_2)$), 31.79 (s, $CH(CH_3)_2$), 22.60 (s, $CH(CH_3)_2$), 20.08 (s, CH_3-ring);. ^{19}F NMR ($CDCl_3$): δ −36.14 (d sept, J(P−F) 1146 Hz, J(F−H) 2.8 Hz).

Preparation of $[RuX_2(\eta^6\text{-cymene})(PCl_3)]$, X = Cl (10), Br (11), I (12). The appropriate dimer compound $[RuX_2(\eta^6\text{-cymene})]_2$ (0.3−0.4 g) was dissolved in dichloromethane (30 mL) and stirred

(70) Neels, A.; Stoeckli-Evans, H.; Plasseraud, L.; Fidalgo, E. G.; Suss-Fink, G. *Acta Crystallogr. C.* **1999**, *55*, 2030–2032.
(71) Ngono, C. J.; Constantieux, T.; Buono, G. *J. Organomet. Chem.* **2002**, *643*, 237–246.
(72) Morse, J. G.; Cohn, K.; Rudolph, R. W.; Parry, R. W. *Inorg. Synth.* **1967**, *10*, 147–156.
(73) Reddy, G. S.; Schmutzler, R. *Z. Naturforsch. B.* **1965**, *20*, 104–109.

with trichlorophosphine (3 mL, excess) for 24 h. The bright red solution was concentrated (10 mL) and petroleum ether (40−60 °C) was added to produce a red precipitate. Crystallization was completed at −30 °C overnight. Filtration and several washings with light petroleum ether (2 × 20 mL) gave a microcrystalline mass which was dried under reduced pressure. The isolated yields of red (**10**), dark red (**11**), and purple (**12**) were 85, 75, and 70%, respectively.

[$RuCl_2(\eta^6$-cymene)PCl_3] (10). (Found: C, 27.58; H, 3.45%; $C_{10}H_{14}Cl_5P_1Ru$ calcd: C, 27.08; H, 3.18%); ^{1}H NMR ($CDCl_3$): δ 1.27 (d, J(HH) 7.0 Hz. 6H, CH(CH_3)$_2$), 2.24 (s, 3H, CH_3-ring), 3.0 (sept, J(HH) 7.0 Hz, 1H, CH(CH$_3$)$_2$), 5.75 (s, 4H, CH-ring); ^{31}P{^{1}H} NMR ($CDCl_3$): δ 141.8 (s, PCl_3); ^{13}C {^{1}H} NMR ($CDCl_3$): δ 113.61 (s, C1-ring), 102.41 (s, C4-ring), 93.12 (d, J(P−C) 7.5 Hz, C2,6-ring), 89.95 (d, J(P−C) 9.0 Hz, C3,5-ring), 30.84 (s, CH(CH$_3$)$_2$), 21.88 (s, CH(CH_3)$_2$), 18.28(s, CH_3-ring).

[$RuBr_2(\eta^6$-cymene)PCl_3] (11). (Found: C, 22.95; H, 2.45%; $C_{10}H_{14}Br_2Cl_3P_1Ru$ calcd: C, 22.56; H, 2.65%); ^{1}H NMR ($CDCl_3$): δ 1.28 (d, J(HH) 7.0 Hz. 6H, CH(CH_3)$_2$), 2.34 (s, 3H, CH_3-ring), 3.14 (sept, J(HH) 7.0 Hz, 1H, CH(CH$_3$)$_2$), 5.71 (s, 4H, CH-ring); ^{31}P{^{1}H} NMR ($CDCl_3$): δ 126.37 (s, PCl_3); ^{13}C {^{1}H} NMR ($CDCl_3$): δ 115.31 (s, C1-ring), 102.88 (s, C4-ring), 93.46 (d, J(P−C) 7.5 Hz, C2,6-ring), 89.98 (d, J(P−C) 9.5 Hz, C3,5-ring), 31.38 (s, CH(CH$_3$)$_2$), 22.04 (s, CH(CH_3)$_2$), 19.09(s, CH_3-ring).

[$RuI_2(\eta^6$-cymene)PCl_3] (12). (Found: C, 18.75; H, 2.05%; $C_{10}H_{14}Cl_3P_1I_2Ru$ calcd: C, 19.17; H, 2.25%); ^{1}H NMR ($CDCl_3$): δ 1.29 (d, J(HH) 7.0 Hz, 6H, CH(CH_3)$_2$), 2.14 (s, 3H, CH_3-ring), 3.38 (sept, J(HH) 7.0 Hz 1H, CH(CH$_3$)$_2$), 5.71 (d, J(HH) 6.5 Hz, 2H, CH-ring), 5.74 (d, J(HH) 6.5 Hz, 2H, CH-ring); ^{31}P{^{1}H} NMR ($CDCl_3$): δ 107.0 (s, PCl_3); ^{13}C {^{1}H} NMR ($CDCl_3$): δ 117.74 (s, C1-ring), 104.60 (s, C4-ring), 94.20 (d, J(P−C) 7.0 Hz, C2,6-ring), 90.79 (d, J(P−C) 9.5 Hz, C3,5-ring), 30.92 (s, CH(CH$_3$)$_2$), 22.48 (s, CH(CH_3)$_2$), 20.18(s, CH_3-ring).

Preparation of [$RuBr_2(\eta^6$-cymene)PBr_3] (13). [$RuBr_2(\eta^6$-cymene)]$_2$ (0.3 g, 0.38 mmol) was dissolved in dichloromethane (30 mL) and stirred with tribromophosphine (3 mL, excess) for 24 h. The bright red solution was concentrated (10 mL) and petroleum ether (40−60 °C) was added to produce a red precipitate. Crystallization was completed at −30 °C overnight. Filtration and several washings with light petroleum ether (2 × 20 mL) gave a red mass identified as [$RuBr_2(\eta^6$-cymene)PBr_3], (0.32 g, 64%). (Found: C, 18.71; H, 2.05%; $C_{10}H_{14}Br_5P_1Ru$ calcd: C, 18.04; H, 2.12%); ^{1}H NMR ($CDCl_3$): δ 1.29 (d, J(HH) 7.0 Hz, 6H, CH(CH_3)$_2$), 2.34 (s, 3H, CH_3-ring), 3.19 (sept, J(HH) 7.0 Hz, 1H, CH(CH$_3$)$_2$), 5.56 (d, J(HH) 6.0 Hz, 2H, CH-ring), 5.71 (d, J(HH) 6.0 Hz, 2H, CH-ring); ^{31}P{^{1}H} NMR ($CDCl_3$): δ 69.8 (s, PBr_3); ^{13}C {^{1}H} NMR ($CDCl_3$): δ 115.50 (s, C1-ring), 101.50 (s, C4-ring), 94.16 (d, J(P−C) 7.0 Hz, C2,6-ring), 89.53 (d, J(P−C) 8.5 Hz, C3,5-ring), 31.53 (s, CH(CH$_3$)$_2$), 22.00 (s, CH(CH_3)$_2$), 18.66 (s, CH_3-ring).

Preparation of [$RuCl_2(\eta^6$-cymene)$(P(NMe_2)_3]$ (14). [$RuCl_2(\eta^6$-cymene)]$_2$ (0.3 g, 0.49 mmol) was dissolved in dichloromethane (30 mL) and stirred with tris(dimethylamino)phosphine (3 mL, 16.5 mmol) for 24 h. The bright red solution was concentrated (10 mL) and petroleum ether (40−60 °C) was added to produce a red precipitate. Crystallization was completed at −30 °C overnight. Filtration and several washings with light petroleum ether (2 × 20 mL) gave a red mass identified as [$RuCl_2(\eta^6$-cymene)$(P(NMe_2)_3)$], (0.33 g, 72%). (Found: C, 40.63; H, 7.05; N, 8.74%; $C_{16}H_{32}Cl_2N_3P_1Ru$ calcd: C, 40.94; H, 6.87; N, 8.95%); ^{1}H NMR ($CDCl_3$): δ 1.30 (d, J(HH) 7.0 Hz, 6H, CH(CH_3)$_2$), 2.15 (s, 3H, CH_3-ring), 2.69 (d, J(PH) 8.5 Hz, 18H, P(NMe_2)$_3$), 3.0 (m, H, CH(CH$_3$)$_2$), 5.11(d, J(HH) 6.0 Hz, 2H, CH-ring), 5.50 (d, J(HH) 6.0 Hz, 2H, CH-ring); ^{31}P{^{1}H} NMR ($CDCl_3$): δ 108.74 (s, $P(NMe_2)_3$); ^{13}C {^{1}H} NMR ($CDCl_3$): δ 112.28 (d, J(P−C) 10.0 Hz, C1-ring), 97.96 (s, C4-ring), 88.86 (d, J(P−C) 8.0 Hz, C2,6-ring), 85.43 (s, C3,5-ring), 39.51 (d, J(P−C) 5 Hz, P(NMe_2)$_3$), 30.44 (s, CH(CH$_3$)$_2$), 27.30 (s, CH(CH_3)$_2$), 18.04 (s, CH_3-ring). ^{13}C{^{1}H}-^{1}H correlations: (1.30, 27.30); (2.15, 18.04); (3.00, 30.44); (5.11, 88.86); (5.50, 85.43).

Preparation of [$RuBr_2(\eta^6$-cymene)$(P(NMe_2)_3]$ (15). [$RuBr_2(\eta^6$-cymene)]$_2$ (0.3 g, 0.38 mmol) was dissolved in dichloromethane (30 mL) and stirred with tris(dimethylamino)phosphine (3 mL, 16.5 mmol) for 24 h. The bright red solution was concentrated (10 mL) and petroleum ether (40−60 °C) was added to produce a red precipitate. Crystallization was completed at −30 °C overnight. Filtration and several washings with light petroleum ether (2 × 20 mL) gave a dark red mass identified as [$RuBr_2(\eta^6$-cymene)$(P(NMe_2)_3)$], (0.29 g, 69%). (Found: C, 34.04; H, 5.64; N, 7.33%; $C_{16}H_{32}Br_2N_3P_1Ru$ calcd: C, 34.42; H, 5.78; N, 7.53%); ^{1}H NMR ($CDCl_3$): δ 1.27 (d, J(HH) 7.0 Hz, 6H, CH(CH_3)$_2$), 2.14 (s, 3H, CH_3-ring), 2.66 (d, J(PH) 8.5 Hz, 18H, P(NMe_2)$_3$, 3.19 (m, H, CH(CH$_3$)$_2$), 4.98 (d, J(HH) 6.0 Hz, 2H, CH-ring), 5.52 (d, J(HH) 6.0 Hz, 2H, CH-ring); ^{31}P{^{1}H} NMR ($CDCl_3$): δ 108.22 (s, $P(NMe_2)_3$); ^{13}C {^{1}H} NMR ($CDCl_3$): δ 112.19 (d, J(P−C) 10.6 Hz, C1-ring), 98.74 (s, C4-ring), 89.85 (d, J(P−C) 5.5 Hz, C2,6-ring), 83.67 (s, C3,5-ring), 39.34 (d, J(P−C) 5.0 Hz, P(NMe_2)$_3$), 30.07 (s, CH(CH$_3$)$_2$), 21.81 (s, CH(CH_3)$_2$), 17.44 (s, CH_3-ring).

Preparation of [$RuI_2(\eta^6$-cymene)$(P(NMe_2)_3]$ (16). [$RuI_2(\eta^6$-cymene)]$_2$ (0.3 g, 0.31 mmol) was dissolved in dichloromethane (30 mL) and stirred with tris(dimethylamino)phosphine (3 mL, 16.5 mmol) for 24 h. The bright red solution was concentrated (ca. 10 mL), and petroleum ether (40−60 °C) was added; a red microcrystalline product formed in the refrigerator at −30 °C overnight. Filtration and several washings with light petroleum ether (2 × 20 mL) gave a red mass identified as [$RuI_2(\eta^6$-cymene)$(P(NMe_2)_3]$, (0.34 g, 85%). ^{1}H NMR ($CDCl_3$): δ 1.25 (d, J(HH) 7.0 Hz, 6H, CH(CH_3)$_2$), 2.15 (s, 3H, (CH_3-ring), 2.65 (d, J(PH) 8.5 Hz, 18H, P(NMe_2)$_3$), 2.8 (m, H, CH(CH$_3$)$_2$), 5.10 (d, J(HH) 6.0 Hz, 2H, CH-ring), 5.80 (d, J(HH) 6.0 Hz, 2H, CH-ring); ^{31}P{^{1}H} NMR ($CDCl_3$): δ 109.48 (s, $P(NMe_2)_3$); ^{13}C{^{1}H} NMR [$CDCl_3$}: δ 112.27 (d, J(P−C) = 12 Hz, C1-ring), 101.98 (s, C4-ring), 91.68 (d, J(P−C) 5 Hz, C2,6-ring), 85.05 (s, C3,5-H-ring), 40.84 (d, J(P−C) 5.0 Hz, P(NMe_2)$_3$), 31.54 (s, (CH(Me)$_2$), 22.94, (s, CH(CH_3)$_2$), 18.13 (s, CH_3-ring).

Computational Details. DFT calculations were based on the single crystal X-ray structure of [$RuBr_2(\eta^6$-cymene)(PF_3)] as a starting point. The ADF 2005 (Amsterdam Density Functional[74]) program has been used to optimize the geometries. For these optimizations, a spin-free relativistic Hamiltonian (the zeroth-order regular approximation, or ZORA[75,76]) has been applied along with the basis sets TZP (triple-ζ singly polarized) and QZ4P (quadruple-ζ with 4 sets of polarization functions) of the

(74) Baerends, E. J.; Autschbach, J.; Berces, A.; Bo, C.; Boerrigter, P. M.; Cavallo, L.; Chong, D. P.; Deng, L.; Dickson, R. M.; Ellis, D. E.; Fan, L.; Fischer, T. H.; Guerra, C. F.; van Gisbergen, S. J. A.; Groeneveld, J. A.; Gritsenko, O. V.; Gruning, M.; Harris, F. E.; van den Hoek, P.; Jacobsen, H.; van Kessel, G.; Kootstra, F.; van Lenthe, E.; Osinga, V. P.; Patchkovskii, S.; Philipsen, P. H. T.; Post, D.; Pye, C. C.; Ravenek, W.; Ros, P.; Schipper, P. R. T.; Schreckenbach, G.; Snijders, J. G.; Sola, M.; Swart, M.; Swerhone, D.; Velde, G. t.; Vernooijs, P.; Versluis, L.; Visser,O.; van Wezenbeek, E.; Wiesenekker, G.; Wolff, S. K.; Woo, T. K.; Ziegler, T., *Amsterdam Density Functional program (ADF)*; Vrije Universiteit Amsterdam: Amsterdam, The Netherlands, 2004; http://www.scm.com.

(75) Lenthe, E. v.; Baerends, E. J.; Snijders, J. G. *J. Chem. Phys.* **1993**, *99*, 4597–4610.

(76) Lenthe, E. v.; Ehlers, A.; Baerends, E. J. *J. Chem. Phys.* **1999**, *110*, 8943–8953.

ADF basis set library and the Becke 88−Perdew 86 non-hybrid generalized gradient approximation (GGA) functional (BP).[77,78] Subsequent calculations of the spin−spin coupling constants were performed with the Gaussian 03[79] (G03) and the ADF programs based on the optimized structures. In the Gaussian calculations we applied the B3LYP[77] hybrid functional along with a scalar relativistic effective core potential (LANL2DZ) for the metal. For Ru, F, C, H, P, Cl, Br, and I, we have used the basis sets LANL2DZ,[80] IGLO-III, 6−311G(d), 6−311G(d), IGLO-III + 6−311G** polarization functions, 6−311G(d), 6−311G(d), and DZVP,[81] respectively. It has been shown in the literature that the IGLO basis allows one to obtain reliable spin−spin coupling constants.[82] For reasons of computational cost we have used this large basis only for P and F and applied smaller basis sets for the other atoms. The main purpose of these calculations was to check that inclusion of exact exchange in the functional does not have an effect on the computed trends for the halide substitutions in the complexes. For the ZORA calculations of spin−spin coupling with ADF at the spin-free (scalar, ZSC) and at the spin−orbit ZORA (ZSO) level of theory we have employed the spin−spin coupling program of the ADF package (which is described in detail elsewhere [45,83]) using the BP functional and the TZP and QZ4P basis sets.

Generally, computations determine the so-called reduced indirect spin−spin coupling constants K for a pair of nuclei, A and B, which are then converted to J-coupling constants by

$$J(\mathrm{A,B}) = \frac{h}{4\pi^2}\gamma_\mathrm{A}\gamma_\mathrm{B}K(\mathrm{A,B}) \quad (1)$$

Here, h is Planck's constant, and γ_A and γ_B are the magnetogyric ratios for atoms A and B. For ^{31}P−^{19}F couplings, this leads to a conversion factor of 4.582 from K in 10^{19} T^2/J to J in units of Hz.

MO contributions[58] to the spin−spin coupling were obtained from the equation for the K-tensor elements

$$K_{(x,y)}(\mathrm{A,B}) = 2\,\mathrm{Re}\sum_i^{occ}\sum_j^{unocc}\frac{\langle\phi_i|\hat{h}_x^{(\mu_\mathrm{A})}|\phi_j\rangle\langle\phi_j|\hat{h}_y^{(\mu_\mathrm{B})}|\phi_i\rangle}{\varepsilon_i-\varepsilon_j} + \sum_i^{occ}\langle\phi_i|\hat{h}_{x,y}^{(\mu_\mathrm{A},\mu_\mathrm{B})}|\phi_i\rangle \quad (2)$$

The μ_A and μ_B superscripts indicate the relevant first and second order perturbation operators with respect to the magnetic moment of nucleus A and B, respectively. One of the first-order operators also contains the perturbation of the molecule's Kohn−Sham potential which is determined self-consistently in the calculations. The ε's are the orbital energies, and the ϕ's the occupied and unoccupied canonical Kohn−Sham orbitals. The second term in eq 2 is the diamagnetic term which was found to be negligible for the coupling constants in the present work. The first term comprises the sum of the paramagnetic, the spin-dipole (SD), the Fermi-contact (FC), and their cross terms and can be written in the AO or another fragment orbital basis as

$$K_{(x,y)}(\mathrm{A,B}) = \sum_r\sum_s P_{rs}^{(\mu_\mathrm{A})}h_{sr}^{(\mu_\mathrm{B})} \quad (3)$$

Here, $P_{rs}^{(\mu_\mathrm{A})}$ is the density matrix perturbed by the magnetic moment of nucleus A, and $h_{rs}^{(\mu_\mathrm{B})}$are the matrix elements due to the perturbation by the other nucleus. A "fragment orbital" analysis was performed using eq 3 which decomposes the calculated K into contributions from pairs r,s of localized fragment orbitals. Details can be found elsewhere.[56,58,62] Further, an analysis using orbitals determined by the NBO 5.0 program[84] was implemented for relativistic ZORA methods, similar to the "natural shielding analysis" originally developed within a nonrelativistic framework by Bohmann et al.[57] This analysis uses eq 3 as a starting point and performs a series of transformation from the AO basis via a basis of "natural bond orbitals" (NBOs) to a basis of natural localized molecular orbitals (NLMOs) as determined by the NBO program. An interface between ADF and NBO 5.0 which has facilitated the implementation has been developed by one of us (J.A.). This new analysis feature was originally developed for the present work using a scalar relativistic theoretical framework (as applied here), which has not previously been published elsewhere. The NLMO/NBO analysis of J-coupling was subsequently extended to ZORA spin−orbit computations by one of the authors. The more general spin−orbit case has been described in detail, and we refer the reader to this paper for details regarding the implementation and the theoretical formalism as well as some applications to validate the method.[85] A corresponding analysis for chemical shifts was also developed recently by us,[86] as well as analyses of first and second hyperpolarizabilities.[87,88] The NBO program yields a set of NLMOs, to each of which the NBO algorithms assign a strongly localized parent NBO. In the present as well as our other analysis papers[62,86−88] we noted that in delocalized electronic structures (often in metal complexes) an automatic NBO generation does not always yield intuitive results (e.g., delocalized bond NLMOs are obtained with a low-occupancy parent lone-pair NBO instead of a bonding NBO). The overall NLMO analysis is generally not much affected by this, but the decomposition into localized and delocalization terms which refers to the NBO basis can be altered. For the complexes studied here, the ADF computations with their rather flexible basis sets initially did not yield the desired set of P−F bonding NBOs. However, the application of the $CHOOSE keyword in the NBO 5.0 computations provided a workaround, and the set of P−F bonding NBOs and the Ru−P NBO were obtained. The subsequent NLMO analysis of J-coupling has been based on this set of NLMOs/NBOs, although we point out that the qualitative aspects of the analysis do not change if the $CHOOSE keyword is not applied (in this case the nature of the NLMOs is easily determined by orbital plots similar to those in Figure 2).

(77) Becke, A. D. *Phys. Rev. A.* **1988**, *38*, 3098–3100.
(78) Perdew, J. P. *Phys. Rev. B.* **1986**, *33*, 8822–8824.
(79) Frisch, M. J. et al. *Gaussian 03*, Revision B.04; Gaussian, Inc.: Wallingford, CT, 2004.
(80) Wadt, W. R.; Hay, P. J. *J. Chem. Phys.* **1985**, *82*, 284–298.
(81) Godbout, N.; Salahub, D. R.; Andzelm, J.; Wimmer, E. *Can. J. Chem.* **1992**, *70*, 560.
(82) Sychrovsky, V.; Grafenstein, J.; Cremer, D. *J. Chem. Phys.* **2000**, *113*, 3530–3547.
(83) Autschbach, J.; Ziegler, T. *J. Chem. Phys.* **2000**, *113*, 936–947.
(84) Glendening, E. D.; Badenhoop, J. K.; Reed, A. E.; Carpenter, J. E.; Bohmann, J. A.; Morales, C. M.; Weinhold, F. *NBO 5.0*; Theoretical Chemistry Institute, University of Wisconsin: Madison, WI, 2001; http://www.chem.wisc.edu/simnbo5.
(85) Autschbach, J. *J. Chem. Phys.* **2007**, *127*, 124106.
(86) Autschbach, J. *J. Chem. Phys.* **2008**, *128*, 164112.
(87) Ye, A.; Autschbach, J. *J. Chem. Phys.* **2006**, *125*, 234101.
(88) Ye, A.; Patchovskii, S.; Autschbach, J. *J. Chem. Phys.* **2007**, *127*, 074104.

Acknowledgment. We thank Johnson-Matthey Chemicals Ltd. for a generous loan of ruthenium trichloride and acknowledge the use of the EPSRC Chemical Database Service at Daresbury.[89] Special thanks to the University of Salford SMT for making travel funds available under the DIASPORA initiative. We thank the Center for Computational Research (CCR) at the University at Buffalo for support. J.A. acknowledges the CAREER program of the National Science Foundation (Grant CHE-0447321) as well as the Petroleum Research Fund for financial support of this research. J.A. and S.Z. thank two of the reviewers for helpful comments and suggestions.

Supporting Information Available: Crystallographic data in CIF format. This material is available free of charge via the Internet at http://pubs.acs.org.

IC800611H

(89) Fletcher, D. A.; McMeeking, R. F.; Parkin, D. *J. Chem. Inf. Comput. Sci.* **1996**, *36*, 746–749.